

Glacier expansion in central Patagonia during the Antarctic Cold Reversal followed by retreat and stabilisation during the Younger Dryas

Monika Mendelová^{a,*}, Andrew S. Hein^a, Ángel Rodes^b, Rachel K. Smedley^c,
Sheng Xu^b

^a*University of Edinburgh, School of Geosciences, Drummond Street, Edinburgh, EH8 9XP, UK*

^b*Scottish Universities Environmental Research Centre, Scottish Enterprise Technology Park, East Kilbride, G75 0QF, Glasgow, UK*

^c*University of Liverpool, Department of Geography and Planning, Chatham Street, Liverpool, L69 7ZT, UK*

Abstract

The spatial-temporal footprint of millennial-scale climate events during the last glacial-interglacial transition can yield insights into the underlying drivers of climate change, but remains poorly resolved in Patagonia. Here, we assess the glacier response to abrupt cold events and palaeolake evolution using geomorphological mapping along with ^{10}Be ages and optically stimulated luminescence ages from near Lago Belgrano (47.9° S) on the eastern side of Monte San Lorenzo. The former Belgrano glacier was sustained by a climatically sensitive ice cap, making the site ideal for investigating the glacier response to abrupt cold reversals. Our data reveal an extensive readvance at 13.1 ± 0.6 ka, consistent with cooling and increased precipitation during the Antarctic Cold Reversal (ACR). Subsequently, ice retreated by

*Corresponding author

Email address: m.mendelova@sms.ac.uk (Monika Mendelová)

at least 10 km and created an ice-dammed proglacial lake in the Belgrano valley. Rapid recession was punctuated by smaller advances/still-stands sufficient to maintain an ice-dam for the palaeolake and deposit a lateral moraine dated at 12.4 ± 0.3 ka during the Younger Dryas (YD). The final withdrawal of glaciers to the mountains allowed the palaeolake to drain and resulted in an Atlantic/Pacific drainage reversal. This marks the final separation of the Patagonian Ice Sheet into the individual ice fields at the YD-Holocene transition. Our data demonstrate the dominant ACR climate signal in central Patagonia, but also reveals a co-occurrence of the northern hemisphere YD signal, albeit of smaller magnitude. The ACR re-advance was primarily climatically controlled, but its relative magnitude was likely a consequence of ice divide migration and ice flow re-routing during the break-up of the Patagonian Ice Sheet.

Keywords:

South America, Quaternary, Antarctic Cold Reversal, Younger Dryas, Cosmogenic isotopes, Luminescence dating, glacial geomorphology, glaciology

1 **1. Introduction**

2 The last glacial-interglacial transition (LGIT, 18 - 11 ka) was charac-
3 terized by the demise of ice-sheets, reorganization of the atmospheric and
4 oceanic systems accompanied by increasing atmospheric CO², and millennial-
5 scale warm/cold events (Denton et al., 2010). The interhemispheric phasing
6 of climate change during this period has generated much debate, in partic-
7 ular the occurrence of the Antarctic Cold Reversal (ACR; ~ 14.6 - 12.8 ka,

8 Lemieux-Dudon et al., 2010) and the northern hemisphere Younger Dryas
9 (YD; $\sim 12.9 - 11.7$ ka; Blunier et al., 1998) climate signals in the southern
10 hemisphere (e.g. Denton et al., 1999; Sugden et al., 2005; McCulloch et al.,
11 2005; Putnam et al., 2010a; Glasser et al., 2012). The relative magnitude
12 and the spatial-temporal footprint of these abrupt events can yield insights
13 into the processes involved in initiation and propagation of climate change,
14 but remains poorly resolved in Patagonia.

15 Patagonia is well-situated for studying this as it intersects the Southern
16 Westerly Winds (SWW), which modulate the global carbon cycle, exert a
17 strong influence on Southern Ocean circulation, and which played an impor-
18 tant role in the LGIT by controlling atmospheric CO_2 (Lamy et al., 2007;
19 Toggweiler et al., 2006; Anderson et al., 2009; Marshall and Speer, 2012). The
20 global climate models predict a poleward shift and strengthening of the SWW
21 in the future, yet also show considerable spatial variability in the magnitude
22 of the strength and position change (Meijers, 2014). Better constraining the
23 timing and magnitude of past glacier fluctuations along latitudinal gradients
24 in the southern mid-latitudes can help to improve our understanding of past
25 climate change, including the role of the SWW, and can help to improve
26 projections of future climate change. Further, examining the consequences
27 of the past rapid climate events on the terrestrial environments, including the
28 cryospheric component, is important for contextualizing present and future
29 climate change in the region.

30 In Patagonia, the ACR signal is well-documented south of 50° S by both
31 glacier chronologies and palaeovegetation records, which reveal glacier ad-
32 vances and cooling coeval with the ACR (Mansilla et al., 2016; Moreno et al.,

33 2012; Björck et al., 2012; García et al., 2012; Moreno et al., 2009; Fogwill
 34 and Kubik, 2005; Strelin et al., 2011; Kaplan et al., 2011; Ackert et al., 2008;
 35 Sugden et al., 2005; McCulloch et al., 2005). Here, subsequent ice retreat
 36 and warming was interrupted by stabilisation of glaciers during the YD (Ka-
 37 plan et al., 2011; Moreno et al., 2009). North of 50° S, the glacier response
 38 to climate during the LGIT remains poorly resolved. Glacier advances/still-
 39 stands during the ACR (Sagredo et al., 2018; Davies et al., 2018; Nimick
 40 et al., 2016) as well as YD (Sagredo et al., 2018; Glasser et al., 2012; Nimick
 41 et al., 2016) have been reported east of the Northern Patagonian Icefield and
 42 on the north-western flanks of Monte San Lorenzo. Many of these glaciers
 43 calved into a large regional palaeolake during most of the LGIT (Davies
 44 et al., 2018; Thorndycraft et al., 2019), and this process together with to-
 45 pographic pinning points on the ice bed likely exerted a strong influence on
 46 their dynamics and response to cold reversals (Davies et al., 2018). In ad-
 47 dition, many exposure ages from moraine boulders previously interpreted as
 48 dating YD advances (Glasser et al., 2012), are considered erroneously young
 49 as a consequence of their submergence in a palaeolake (Thorndycraft et al.,
 50 2019). In some cases, the relationship between the dated moraines (e.g.
 51 Nimick et al., 2016) and palaeolakes remains unclear. Where YD moraines
 52 have been dated, they are based on a limited number of exposure ages (\leq
 53 2) (Sagredo et al., 2018; Glasser et al., 2012). Thus, firm dating of YD ice
 54 limits has not yet been achieved.

55 Terrestrial palaeovegetation proxies from central Patagonia (49° S - 44°
 56 S) either: (i) do not document any clear changes from which an ACR or YD
 57 signal can be inferred (Haberle and Bennett, 2004; Bennett, 2000; Lumley

58 and Switsur, 1993; Markgraf et al., 2007; de Porras et al., 2014, 2012; Iglesias
 59 et al., 2016), or (ii) suggest persistence of cold/cool and wet conditions from
 60 about 16 ka to 11.8 ka (Villa-Martínez et al., 2012). Only one terrestrial
 61 record so far suggests increased precipitation coeval with the ACR, based on
 62 an increase of cold-resistant hygrophilous taxa between 14 ka and 13.5 ka
 63 (Henríquez et al., 2017). This is supported by pollen analysis on a marine
 64 core recovered from offshore of Chile (46° S; MD07-3088, Montade et al.,
 65 2013). The absence of the ACR and/or YD signal in many records might
 66 be masked by high climate variability during the LGIT, combined with
 67 the effects of local climate and/or insensitivity of proxies to minor cooling
 68 (Markgraf et al., 2007; Villa-Martínez et al., 2012; Mendelova et al., 2017).

69 The aim of this study is to assess the glacier response to cold reversals
 70 during the LGIT in the Belgrano and Lacteo valleys on the eastern side of
 71 Monte San Lorenzo. We selected this site because the relatively small San
 72 Lorenzo ice cap would have been more sensitive to climate change than the
 73 larger Patagonian icefields. At its maximum extent during the LGIT, the
 74 former Belgrano glacier had a land-terminating margin rather than a calving
 75 margin, and thus glacier fluctuations here are more likely to reflect changes
 76 in climate. These characteristics make the site ideal for investigating the
 77 regions glacier response to abrupt millennial-scale cooling events during the
 78 LGIT. We use geomorphological mapping, cosmogenic ^{10}Be surface exposure
 79 dating and optically-stimulated luminescence (OSL) analysis to determine
 80 the timing of 1) major glacier re-advances/stillstands during the LGIT, and
 81 2) the formation and evolution of palaeolakes in the valleys. Our mapping
 82 and chronology gives insight on the processes involved in the break-up of the

83 former Patagonian Ice Sheet (PIS) and rates of deglaciation.

84 **2. Study area and previous work**

85 *2.1. Physical setting*

86 Monte San Lorenzo (3706 m, Chilean name: Monte Cochrane) is an iso-
87 lated massif located ~ 80 km east of the main spine of the Patagonian Andes
88 (Figs. 1 and 2). At this latitude, the main chain of the Andes exhibits a
89 tectonic depression, which separates Monte San Lorenzo massif from the Pa-
90 cific coast, and the Northern Patagonian Icefield from the Southern Patag-
91 onian Icefield. The Lago Belgrano valley is a relatively small, low gradient,
92 high elevation valley at over 850 m asl. This contrasts with the large over-
93 deepened basins to the north and south (e.g. Lago Puyeredón, 150 m) that
94 have been eroded to below sea level (Murdie et al., 1998). The low gradient
95 Belgrano valley also contrasts with mountain valleys on the northern and
96 western flanks of Monte San Lorenzo, which have steeper elevation profiles
97 as they descend to low elevations ($\sim 500 - 200$ m asl) within tens of km of
98 the mountain. San Lorenzo is part of the Patagonian Batholith intrusion
99 (Ramos and Kay, 1992; De Arellano et al., 2012), and is the main source of
100 granitic erratics that are found in the Belgrano valley.

101 The precipitation-bearing SWW have a dominant influence on climate
102 and sustain the present day ice-fields and glaciers. Westerly precipitation
103 can reach 5,000 - 10,000 mm a^{-1} on the western side of the Andes and
104 falls to less than 300 mm a^{-1} tens of km downwind of the mountain front
105 (Garreaud et al., 2013). As a consequence of the topographic depression, the
106 Monte San Lorenzo massif is the first orographic barrier to the SWW, and

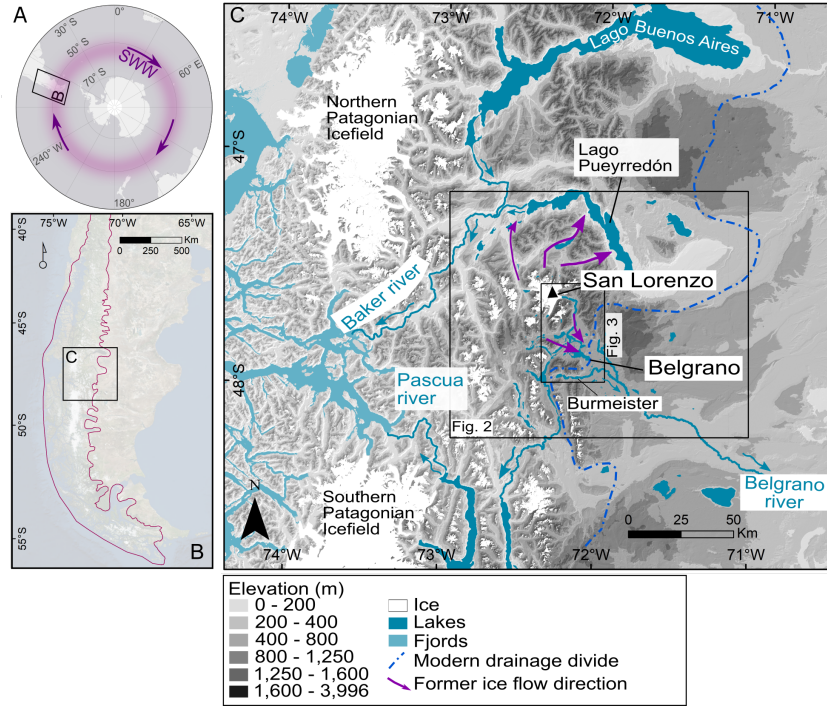


Figure 1: A) Location of Patagonia in the southern hemisphere with approximate location of the Southern Westerly Winds. B) Location of the study area in Patagonia, with an approximate extent of the Patagonian Ice Sheet at the global Last Glacial Maximum (pink line). Image: ESRI World Imagery. C) Map of central Patagonia showing contemporary ice fields and ice caps (outlines were downloaded from the GLIMS database (Falaschi et al., 2017; De Angelis et al., 2015)), modern drainage divide and location of Monte San Lorenzo and Lago Belgrano valley. Magenta arrows indicate former ice discharge routes from the San Lorenzo. Basemap: Shuttle Radar Topography Mission DEM.

107 has a transitional maritime to continental climate (Falaschi et al., 2013).

108 The San Lorenzo massif sustains four valley glaciers and several smaller
 109 ice bodies covering a total area of $\sim 139 \text{ km}^2$ (Falaschi et al., 2013). The
 110 snowline is estimated to be $\sim 1700 - 1750 \text{ m a.s.l}$ on the western side and
 111 about 100 m higher on the eastern side of the massif (Falaschi et al., 2013).

112 All glaciers of the San Lorenzo massif and Lago Belgrano drain westward to
113 the Pacific Ocean via rivers, which exploit the gap in the mountain chain
114 (Fig. 2). The drainage divide is located east of Lago Belgrano, and Lago
115 Burmeister (~ 900 m asl; Fig. 2) is over the divide and instead drains east-
116 ward to the Atlantic Ocean via the Río Belgrano. During glacial cycles, the
117 build-up of ice along the Andean mountain chain blocked Pacific drainage
118 pathways, causing large-scale drainage reversals. The break-up of the Patag-
119 onian Ice Sheet is thus associated with large-scale drainage reversals across
120 many parts of Patagonia (Caldenius, 1932; Turner et al., 2005; Thorndycraft
121 et al., 2019).

122 *2.2. Previous work*

123 During full glacial conditions, the San Lorenzo ice cap coalesced with the
124 larger PIS (Caldenius, 1932; Wenzens, 2005; Glasser et al., 2005; Mendelova
125 et al., 2019). Ice from the San Lorenzo centre discharged northwards to join
126 the Lago Puyerrredón outlet glacier and south-eastwards into the Belgrano
127 valley (Fig. 1 C; Wenzens, 2002). The Belgrano glacier had additional ice
128 contribution from accumulation areas on the mountains to the west and south
129 of Lago Belgrano.

130 Following disintegration of the Lago Puyerrredón lobe, ice on the northern
131 and western flanks of San Lorenzo was largely confined to the mountain
132 valleys (Davies et al., 2018; Martin et al., 2019; Sagredo et al., 2018). Here,
133 advances of the Tranquilo and Calluqueo glaciers were dated at 13.8 ± 0.5
134 ka and 13.2 ± 0.2 ka, respectively, coeval with the ACR (Fig. 2; Sagredo
135 et al., 2018; Davies et al., 2018). At this time, the Calluqueo glacier calved
136 into a palaeolake, and part of the moraine was subaqueous (Davies et al.,

2018). YD stabilisation is suggested by a couple of exposure ages from inset
moraines in both valleys (Fig 2; 12.5 ± 0.4 and 11.6 ± 0.4 ka in the Tranquilo
valley (Sagredo et al., 2018), and 12.9 ± 0.8 and 12.0 ± 0.5 in the Salto valley
(Glasser et al., 2012)).

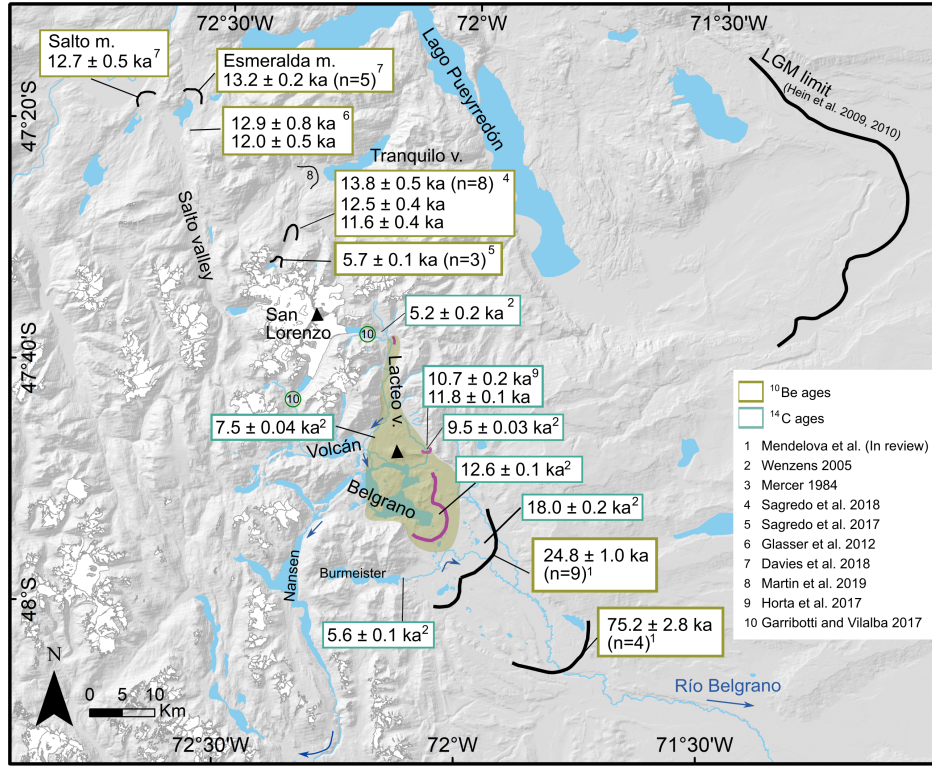


Figure 2: Map showing Monte San Lorenzo, Lago Belgrano and Lacteo valleys, along with published chronologies (black curves indicate dated ice margins). Where more than 2 ages exist for a landform, uncertainty-weighted means with 1σ standard deviation are presented. Otherwise, individual ages are given with 1σ uncertainty (internal in case of ^{10}Be ages). Green shading indicates our study area, and ice margins dated in this study are highlighted in pink. Glacier outlines were downloaded from the GLIMS database (Falaschi et al., 2017; De Angelis et al., 2015). River drainage directions are indicated with blue arrows.

141 The Belgrano glacier reached its full last glacial extent at 75.0 ± 2.8 ka
 142 based on ^{10}Be exposure ages from outwash cobbles (Fig. 2; Mendelova et al.,
 143 2019). This early maximum suggests that an independent ice mass developed
 144 on San Lorenzo early in the last glacial cycle toward the end of MIS 5. A
 145 second major advance deposited the Menelik moraines dated using ^{10}Be ages
 146 at 24.7 ± 1.0 ka (Fig. 2; Mendelova et al., 2019), coeval with the global Last
 147 Glacial Maximum (gLGM).

148 The Late Glacial history at Lago Belgrano is only constrained by two
 149 minimum radiocarbon ages of 12.6 ± 0.06 cal ka BP and 9.5 ± 0.04 cal ka
 150 BP (Wenzens, 2005; Table 1 and Fig. 2). With the exception of the Tranquilo
 151 valley, where Sagredo et al. (2018) dated an advance to $5.7 \text{ ka} \pm 0.1 \text{ ka}$ using
 152 ^{10}Be , our knowledge of the Holocene dynamics of the San Lorenzo glaciers
 153 is limited to minimum radiocarbon ages and lichenometry (Garibotti and
 154 Villalba, 2017; Mercer, 1984; Wenzens, 2005). In the Lacteo valley (Fig. 2),
 155 Wenzens (2005) obtained an age of 7.5 ± 0.04 cal ka BP from a kettle hole,
 156 and further up valley, Mercer (1984) obtained a maximum age of 5.2 ± 0.2
 157 cal ka BP from an overridden tree incorporated within a moraine 5 km from
 158 the present day margin of the Lacteo glacier. Wenzens (2005) obtained a
 159 minimum age of 5.6 ± 0.06 cal ka BP from a kettle hole within the moraines
 160 bounding Lago Burmeister (Fig 2). Horta et al. (2017) proposed a palaeolake
 161 in the Belgrano valley at 900 - 920 m a.s.l. between 11.7 and 10.8 ka on the
 162 basis of two radiocarbon ages from lacustrine deposits (Table 1 and Fig 2).

163 Geomorphological mapping of the valleys on the eastern side of Monte San
 164 Lorenzo along with a robust chronology will allow us to assess the response
 165 of this small ice cap to climate fluctuations during the ACR and YD, and

166 will provide insight on the overall pattern and rate of deglaciation.

167 **3. Methods**

168 In this study, we focus on a moraine system that bounds the eastern end
169 of Lago Belgrano, here informally named the Belgrano moraine system, and
170 the area to the north, including the Lacteo valley (Figs. 2 and 3). The
171 two older moraine systems in the Belgrano valley (Fig. 2) and associated
172 chronologies are described by Mendelova et al. (2019).

173 Geomorphological mapping was done from high resolution optical satellite
174 imagery (2.5 m to sub-meter) distributed by the ESRITM World Imagery
175 service, 10 m Sentinel-2 imagery and Google Earth. ALOS PALSAR (12.5
176 m) and Shuttle Radar Topography Mission (30 m) digital elevation models
177 were used to aid landform identification. Geomorphological features were
178 mapped following established criteria (e.g. Glasser et al., 2008; Darvill et al.,
179 2014; Bendle et al., 2017; Martin et al., 2019). Mapping was field-checked
180 during two field campaigns in 2016 and 2018.

181 Published ^{10}Be ages from Patagonia described in this paper were recal-
182 culated using the protocol outlined in section 3.1.2, and ages are presented
183 as uncertainty (internal) weighted means with 1 σ standard deviation per
184 moraine. Published radiocarbon ages (Table 1) were recalibrated using the
185 OxCal online calibration program (version 4.3; Bronk Ramsey, 2009) and the
186 southern hemisphere calibration curve (SHCal13, Hogg et al., 2013). The cal-
187 ibrated median ages (95.4 % confidence interval) are presented as "cal. ka
188 BP", rounded to the nearest 100 a.

189 3.1. Surface exposure dating

190 3.1.1. Sampling

191 For cosmogenic nuclide analysis, we collected samples from the top centre
192 of large boulders embedded in the moraine crests using hammer and chisel
193 (Gosse and Phillips, 2001; Darvill, 2013). We targeted granitic boulders that
194 showed minimal surface erosion, and appeared stable. We sampled four to
195 six boulders per moraine limit (cf. Putkonen and Swanson, 2003). Three
196 samples were collected from boulders and cobbles deposited atop bedrock
197 outcrops along a transect in the Lacteo valley to date deglaciation of the
198 valley. Additionally, we collected two surface samples from beach gravels on
199 former shorelines. The shoreline samples consisted of an amalgamation of
200 30-40 quartz-rich pebbles (2-4 cm).

201 Sample locations were recorded with a handheld Garmin GPS with a
202 reported accuracy of 3 - 5 m. Topographic shielding was measured in the
203 field using a compass and clinometer, and shoreline altitudes were cross-
204 checked with a barometric altimeter. Sample details are presented in Table
205 2 and sample locations are shown in Figure 3.

206 The samples were crushed whole, except sample RV1609, which was cut
207 horizontally to reduce its thickness. Subsequently, the samples were sieved
208 to obtain the sand fraction and then prepared as ^{10}Be AMS targets at two
209 different cosmogenic nuclide laboratories: the Natural Environment Research
210 Council's Cosmogenic Isotope Analysis Facility (NERC-CIAF), and the Uni-
211 versity of Edinburgh's Cosmogenic Nuclide Laboratory. All Accelerator Mass
212 Spectrometry (AMS) measurements were conducted at the Scottish Universi-
213 ties Environmental Research Centre (SUERC) AMS Facility. Sample prepa-

214 ration for cosmogenic nuclide analysis is described in Mendelova et al. (2019).

215 3.1.2. Age calculations

216 ^{10}Be ages were calculated using the online exposure age calculator de-
217 scribed by Balco et al. (2008), version 3, with a local ^{10}Be production rate
218 for Patagonia (Kaplan et al., 2011), derived from the ICE-D online database
219 (<http://calibration.ice-d.org/>). Ages presented here (Table 3) use the
220 time-dependent Lm scaling scheme of Lal (1991) modified by Stone (2000).
221 The ages decrease by 0.5 % if calculated using the New Zealand production
222 rate of Putnam et al. (2010b) and decrease by 6% with the global production
223 rate of Borchers et al. (2016). Summary statistics for each moraine are given
224 in Table 3. We base our discussion on the uncertainty-weighted means and
225 1 σ standard deviation.

226 No correction is applied for shielding by vegetation or snow because
227 the moraines are sparsely vegetated by grasses with the exception of some
228 Nothofagus trees scattered on the lateral moraines in the Lacteo valley. Given
229 high winds and low precipitation, we expect the snow cover to be minimal
230 and short-lived in the Belgrano valley. Closer to the mountain front, snow
231 cover would be more persistent, but boulders perched on moraines are likely
232 to sit above the snowpack where they can be blown free of snow. Exposure
233 ages assume zero erosion, although rates of 0.2 mm ka^{-1} have been estimated
234 nearby (Hein et al., 2017; Douglass et al., 2007). Including this rate would
235 increase ages by less than 1%, which is within analytical uncertainties.

236 The moraine boulder ages are interpreted to date moraine stabilisation
237 following ice withdrawal, and thus the ages provide a minimum age for the ice
238 advance. The cosmogenic nuclide ages are considered minimum ages, given

239 the potential for post-depositional processes (e.g. erosion and exhumation
240 of boulders) that could affect surface exposure. That said, we acknowledge
241 inheritance could interfere with this assumption, and this is discussed explic-
242 itly.

243 The exposure ages from shorelines are interpreted to date the abandon-
244 ment (stabilisation) of the shoreline, and therefore dropping of the lake level.
245 We assume that wave action cuts into existing sediment and subjects in-
246 dividual clasts to surface erosion such that inheritance is negligible. This
247 assumption is, however, difficult to test without several samples from each
248 shoreline. Our approach of amalgamating many surface clasts should go
249 some way toward minimising the influence of inheritance on the final ^{10}Be
250 concentration of the sample.

251 3.2. OSL dating

252 We collected two samples for luminescence dating from laminated silt
253 and sand sediments interpreted as glaciolacustrine deposits. We interpret
254 the ages to date the deposition of these sediments, and they should therefore
255 give a minimum age for the development of a palaeolake.

256 Samples for luminescence dating were collected in opaque tubes and pre-
257 pared for analysis under subdued lighting conditions following the procedure
258 of Smedley et al. (2016). To calculate the environmental dose-rate through-
259 out burial for each sample, U, Th and K concentrations were measured for \sim
260 80 g of the bulk sediment sample using high-resolution gamma spectrometry.
261 Environmental dose-rates determined for samples RV1801 (212 - 250 μm)
262 and LBSH1801 (125 - 180 μm) are shown in Table S1. Coarse grains of K-
263 feldspar were used to determine equivalent doses (D_e) using 300 μm -diameter

264 single-grain discs and a Risø TL/OSL DA-15 automated single-grain system
 265 equipped with a $^{90}\text{Sr}/^{90}\text{Y}$ beta source (Bøtter-Jensen et al., 2003). Single
 266 aliquot regenerative dose (SAR) protocols (Murray and Wintle, 2000) were
 267 used for the post-IR IRSL analyses performed at 225 °C (Thomsen et al.,
 268 2008), termed the pIRIR₂₂₅ signal. Grains from both samples were used
 269 for dose-recovery experiments and successfully recovered a given dose within
 270 10 % using the pIRIR₂₂₅ signal. Fading experiments reported g-values of
 271 -0.4 ± 0.7 %/decade (RV1801) and -1.0 ± 0.7 %/decade (LBSH1801), which
 272 suggests that no fading correction was required for the pIRIR₂₂₅ signal. D_e
 273 values were calculated from all grains passing all the screening criteria. The
 274 minimum age model (MAM; Galbraith et al., 1999; Galbraith and Laslett,
 275 1993) was applied to determine an age for the samples as the asymmetrical
 276 D_e distributions suggested the samples were partially bleached prior to burial
 277 (Fig. S1). The D_e values were then divided by the environmental dose-rates
 278 to determine an age for each sample (Table S1). See the supplementary
 279 material for full details on the luminescence dating in this study.

280 **4. Results**

281 *4.1. Geomorphology*

282 The Belgrano moraine system (Figs. 4 and 5) is comprised of up to 10
 283 arcuate moraine ridges with undulating crests. The outermost moraine ridge
 284 is subdued at 3 m height and a slope of 5°. The morphology of this moraine
 285 ridge may indicate that the glacier occupied this position for a shorter time or
 286 the moraine ridge degraded post-deposition. The next two moraine ridges are
 287 the most prominent and continuous with about 10 m in height and slopes up

288 to 22°. Inboard of these the moraines appear more hummocky with occasional
289 inter-morainic depressions. The inner moraine ridges are again distinct with
290 10 m in relief. The moraines are vegetated by grasses and short shrubs with
291 patches of exposed coarse gravel and large cobbles. We sampled four boulders
292 on the innermost moraine ridges, and four boulders on the outermost subdued
293 moraine ridge (Fig. 4). A broad glaciofluvial outwash plain grades from the
294 moraines toward the east with preserved braided channels.

295 The Belgrano moraines cross-cut older recessional moraines (cf. Mende-
296 lova et al., 2019) on the northeastern side of the lake (Figs. 5 and 6), in-
297 dicating that the Belgrano moraines were deposited by a re-advance of the
298 Belgrano glacier, rather than a still-stand during overall deglaciation. The
299 location of the older recessional moraines suggest that after the culmination
300 of the gLGM advances/still-stands, the Belgrano glacier withdrew and was
301 largely confined to its trough prior to the re-advance.

302 To the north of the Belgrano moraines exists a series of latero-terminal
303 moraines (Fig. 5), here informally termed the Rincon moraines, which were
304 deposited by the Lacteo glacier. The Rincon moraines occupy the same
305 morphostratigraphic position as the Belgrano moraines. They are situated
306 on the northern slope of Monte Leon and in the gap between Monte Leon
307 and the NE valley side. The terminal moraine ridges (Figs. 7 A and B)
308 are discontinuous and have been dissected by several meltwater channels
309 up to 40 m in width. We collected four ^{10}Be samples from the terminal
310 moraine ridges. A glaciofluvial outwash grades from the moraines toward
311 the southeast, extending for about 6 km until it merges with the Belgrano
312 outwash. Immediately outboard of the Rincon moraines, the outwash terrace

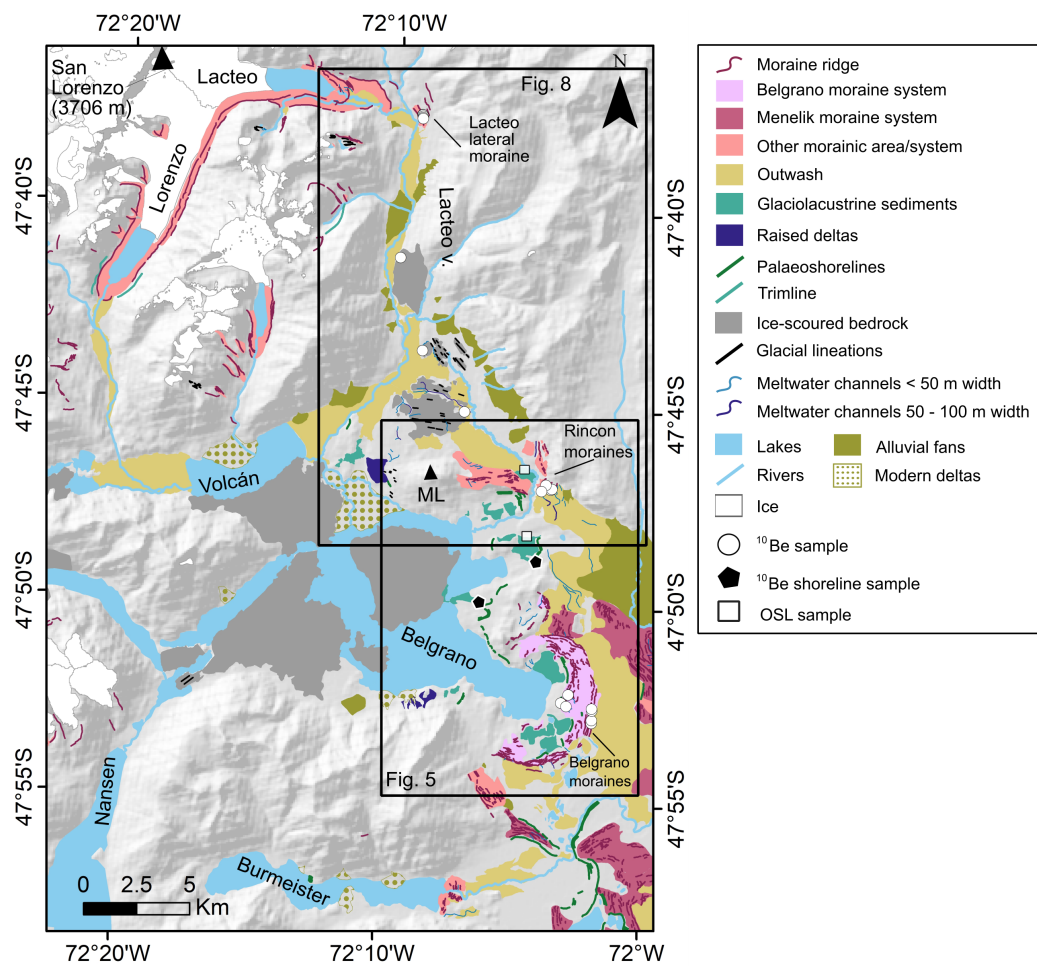


Figure 3: The geomorphological map of the Belgrano and Lacteo valleys. Sample locations are also shown (white circles). The hillshade basemap was derived from the Shuttle Radar Topography Mission Digital Elevation Model.

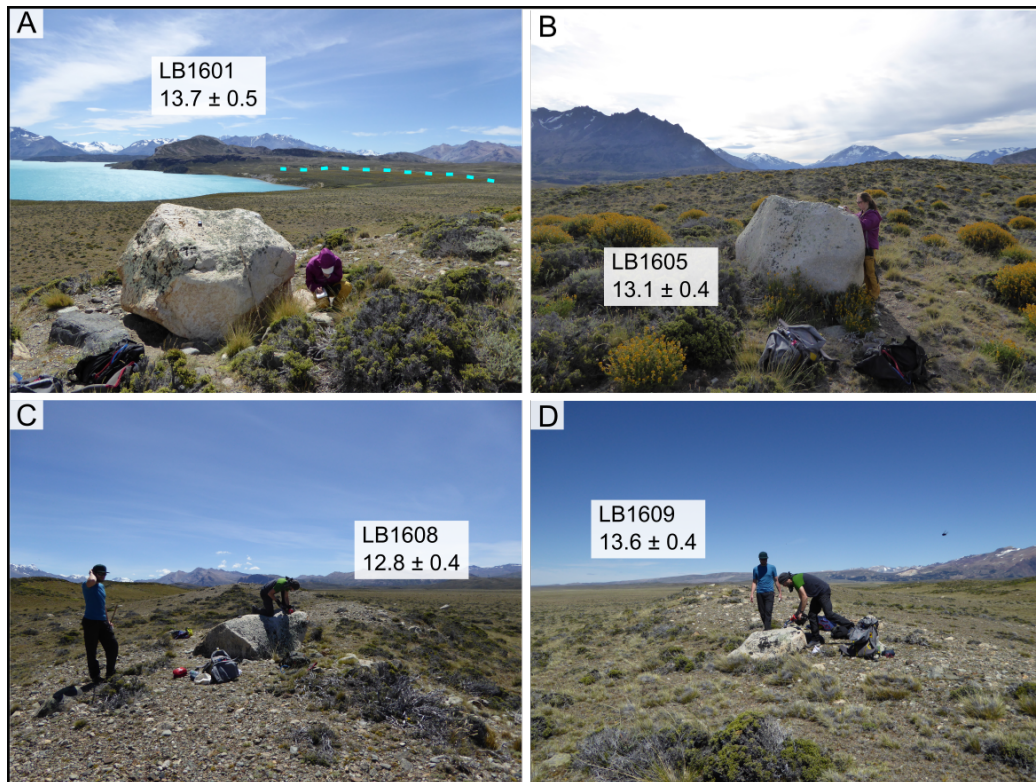


Figure 4: Examples of moraine boulders sampled for surface exposure analysis. (A & B) Boulders on the innermost Belgrano moraine, a former shoreline is visible in the background (A, dashed line). (C & D) Boulders on the outermost Belgrano moraine.

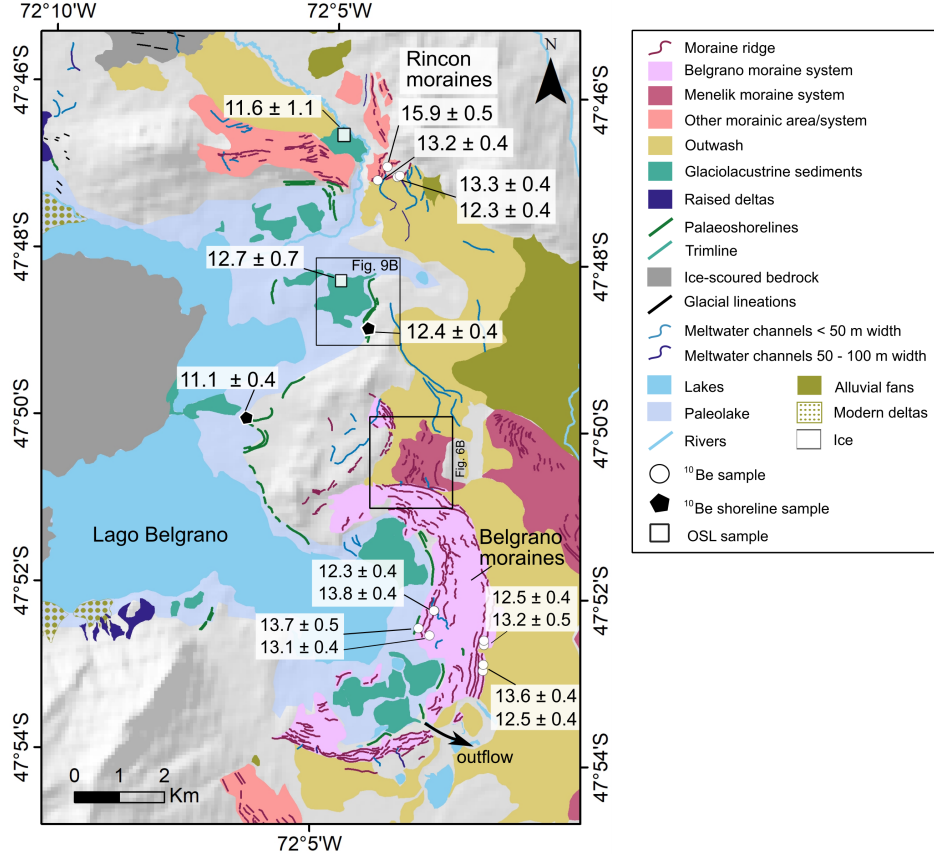


Figure 5: Enlarged geomorphology map showing the Belgrano and Rincon moraines. The locations of moraine boulder samples, shoreline samples and OSL samples collected from glaciolacustrine deposits are also shown. The area where the Belgrano moraines cross-cut older recessional moraines is indicated with a box (Fig.6 B). The ^{10}Be ages presented here are individual ages with 1σ internal uncertainty. The approximate area of the palaeolake is indicated. This is based on 882 m asl elevation extracted from an SRTM DEM with resolution of 30 m.

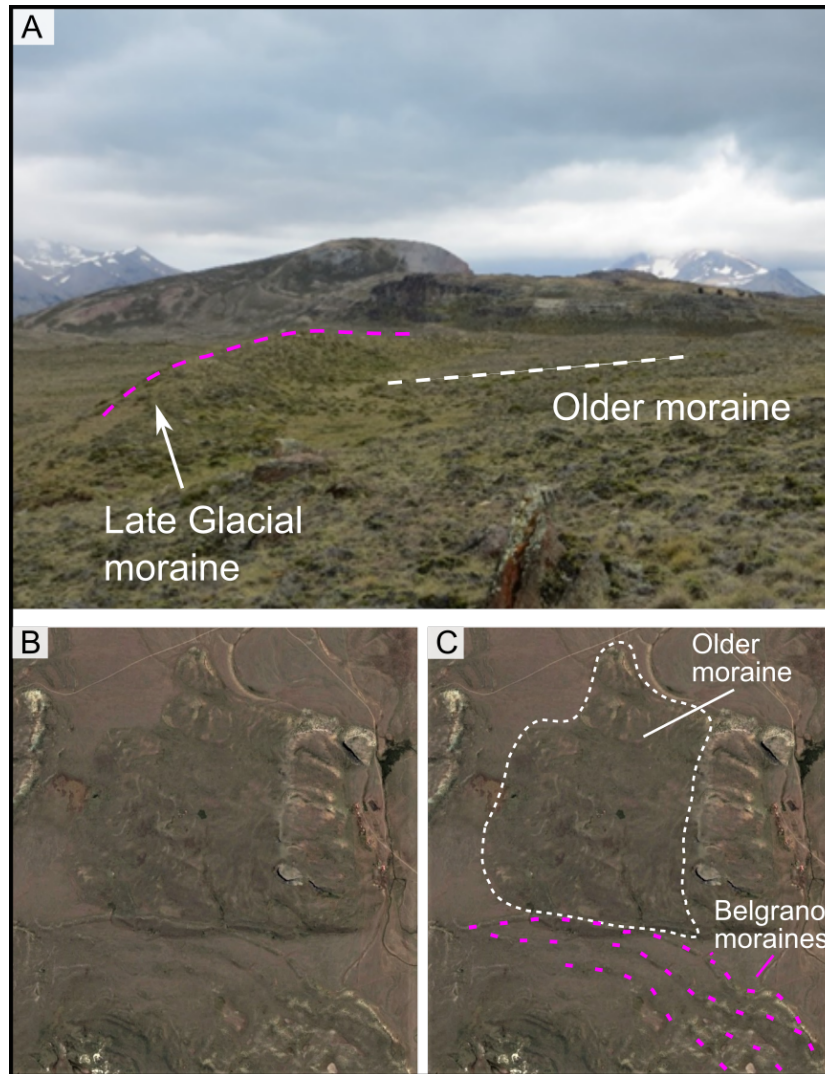


Figure 6: (A) Photograph showing the area where the Belgrano moraines cross-cut older moraines. (B & C) Satellite images showing the cross-cutting relationship (Image: Google Earth).

313 has been incised by meltwater channels creating a series of stepped terraces.

314 About 20 km upvalley from the Rincon moraines, and 7 km from the
315 present day margin of the Lacteo glacier, there is a prominent multi-crested
316 lateral moraine perched 45 - 60 m above the valley floor (Fig. 8). This lateral
317 moraine spans a width of 100 m with several distinct crests (2-5 m in relief)
318 that are rich in surface boulder (Figs. 7 C & D). Given that the lateral
319 moraine is only 45 - 60 m above the valley floor, we interpret the moraine to
320 be morphostratigraphically younger than the Rincon moraines. We collected
321 six ^{10}Be samples from this lateral moraine.

322 4.1.1. *Palaeo shorelines*

323 A major palaeo-shoreline at 882 - 885 m asl can be traced along the
324 southern and northern shores of Lago Belgrano and on the ice-proximal side
325 of the Belgrano moraines (Figs. 5 and 9). This shoreline is most prominent
326 on the eastern end of the lake where wave action from westerly winds would
327 have been at its greatest. Here, the shoreline is etched into bedrock and
328 sediment, but traces of the shoreline were observed at least 10 km upvalley,
329 and thus the lake covered a substantial area. Higher shorelines can also be
330 found (e.g. at ~ 889 - 892 m asl.), but are spatially restricted, and could
331 indicate a higher palaeolake level or smaller ice-marginal lakes.

332 The palaeolake drained eastward to the Atlantic via an outflow through
333 the Belgrano moraines at ~ 883 m asl (Fig. 5). The palaeolake Belgrano
334 existed when the drainage route through to Lago Nansen (Fig. 2) was blocked
335 by ice. The lowering of the lake indicates the loss of this ice dam, and the
336 retreat of ice back into the high mountains. Sediment from this lake, mainly
337 laminated silt to sandy-silts, are preserved at several locations throughout

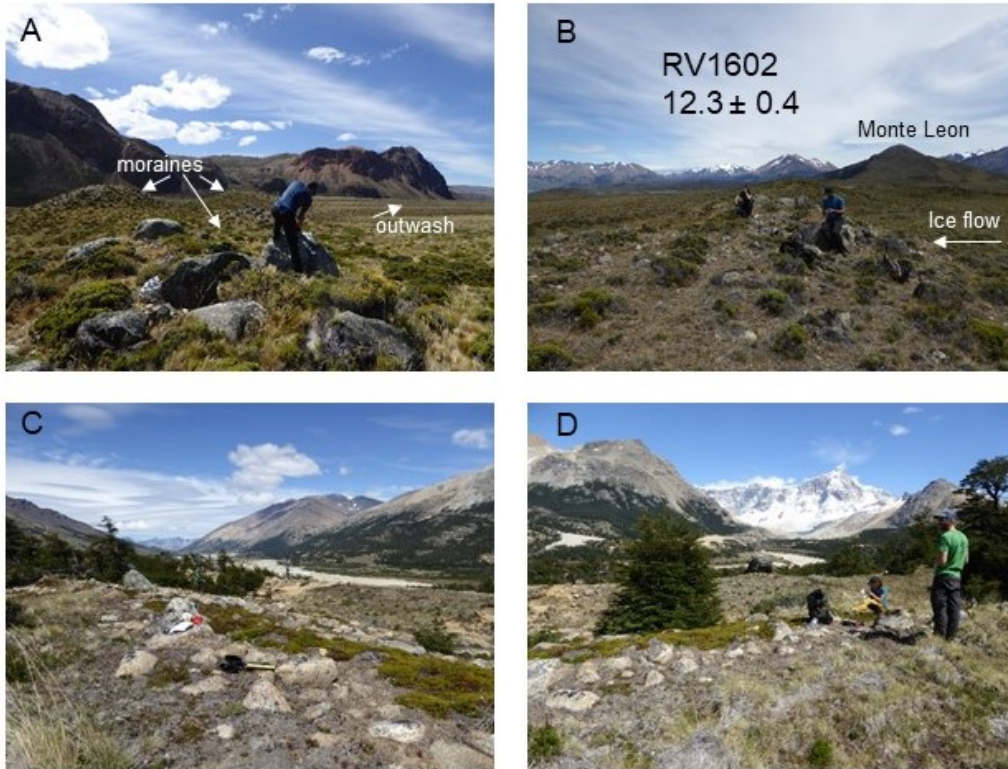


Figure 7: (A & B) Photographs showing the Rincon moraines and an outwash plain grading from the moraines to the SE. The outwash terrace was incised by meltwater creating a series of stepped terraces. (C & D) Photographs showing the multi-crested lateral moraine in the Lacteo valley, about 7 km from the present day margin of the Lacteo glacier.

the basin. We collected two ^{10}Be samples from the 882 - 885 m asl shorelines (Figs. 5 and 9). The shorelines in this area take a form of a flat gravel beach berm up to 30 m wide. On the surface they are composed of medium well-sorted gravel (clasts up to 4 cm) and little to no vegetation.

OSL sample LBSH1801 (850 m; Figs. 5 and 9) came from a road exposure of silty sediments that infill the valley bottom directly below the the 882 - 885 m asl shoreline. The sediments are laminated sandy silts with water escape features. Numerous boulders and cobbles are visible on the surface of the deposit but less frequently within the exposure. We interpret these sediments as glaciolacustrine sediments, which relate to the 882 - 885 shorelines.

The second OSL sample (RV1801, 893 m; Fig. 5) came from a horizontally - laminated silt and sand deposit situated inboard of the Rincon moraines in the Lacteo valley. We interpret this deposit as glaciolacustrine sediments from a smaller proglacial lake that formed in the Lacteo valley and was independent to the Belgrano palaeolake.

4.2. Chronology

4.2.1. Timing of the readvance

The Belgrano and Rincon moraines are contemporaneous and represent a readvance of the Belgrano and Lacteo glaciers. ^{10}Be ages from the outermost Belgrano moraine ridge range from 12.5 ± 0.4 ka to 13.6 ± 0.4 ka, and yield a weighted mean of 13.0 ± 0.5 ka. The innermost moraines yield ages ranging from 12.3 ± 0.4 ka to 13.8 ± 0.4 ka, with a weighted mean of 13.2 ± 0.6 ka (Table 3, Figs. 5 and 10). The ages from the inner and outer moraine ridges are statistically indistinguishable. Within the dating resolution, we cannot distinguish the individual advances, instead, we group the ages together to

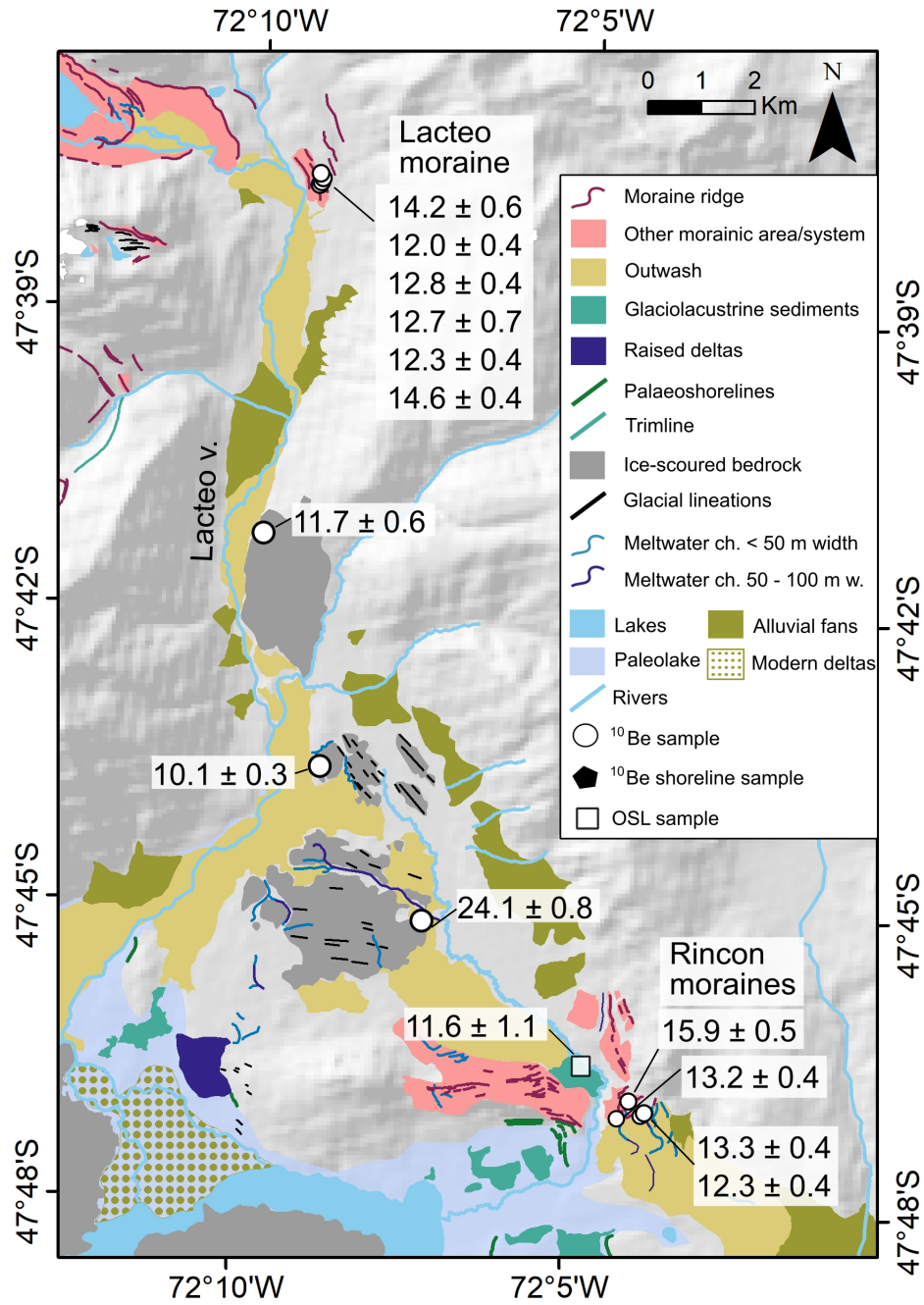


Figure 8: Enlarged geomorphology map of the Lacteo valley. Locations of samples collected from the Lacteo lateral moraine and along a transect in the valley are shown. The ^{10}Be ages presented here are individual ages with 1σ internal uncertainty.

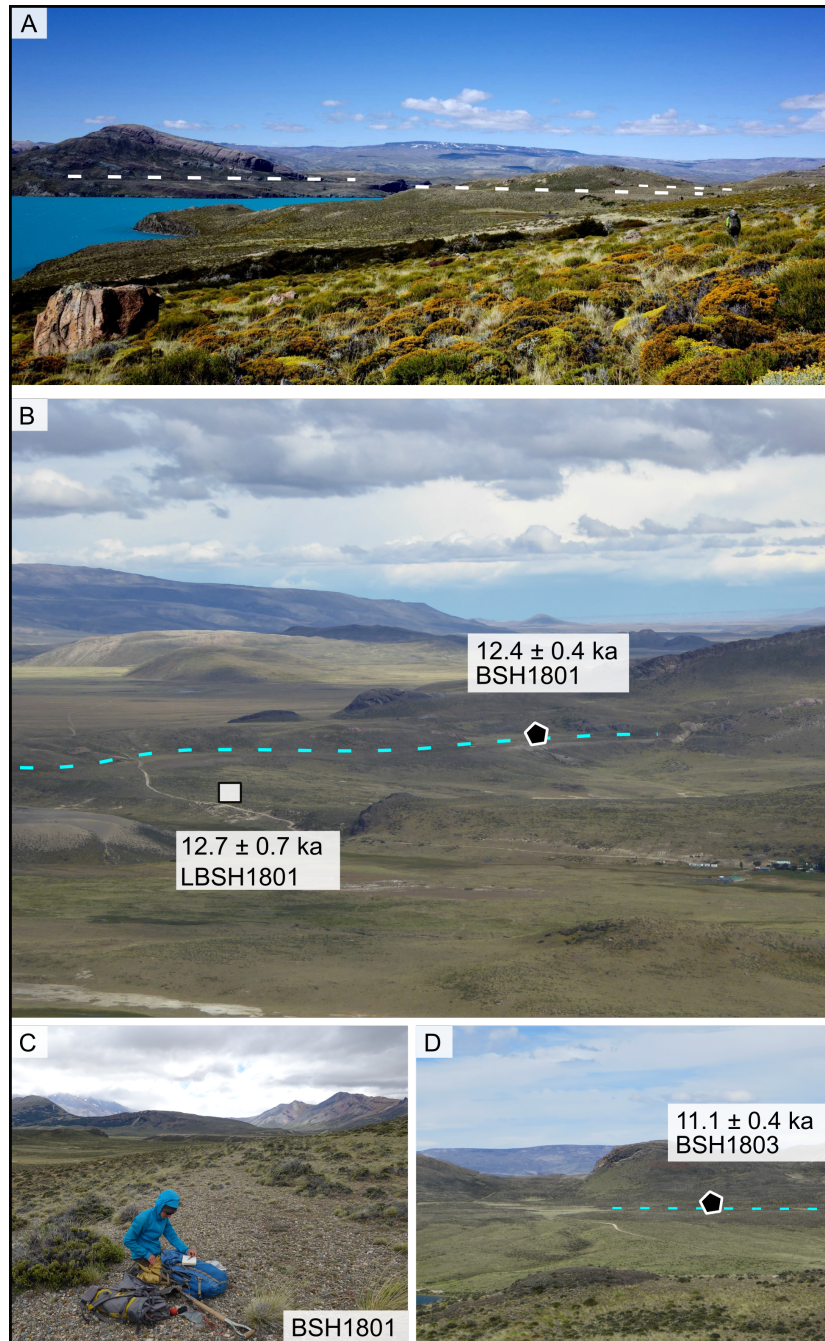


Figure 9: (A) Photograph showing raised shorelines above the modern Belgrano lake. (B) Photograph showing a palaeoshoreline with the location of surface exposure (black hexagon) and OSL (square) samples. The valley bottom below the shoreline is infilled with glaciolacustrine sediments. (C) Photograph showing the surface of a shoreline where sample BSH1801 was taken. (D) Photograph of a shoreline where sample BSH1803 was taken.

363 date the readvance at 13.1 ± 0.6 ka (weighted mean). The Rincon moraines
364 yielded similar ages of 12.3 ± 0.4 , 13.3 ± 0.4 , and 13.2 ± 0.4 ka, and a
365 weighted mean age of 12.9 ± 0.4 ka (Figs. 5 and 10 C). We excluded one
366 sample with an older age of 15.9 ± 0.5 ka as an outlier.

367 4.2.2. *Ice withdrawal and stabilisation*

368 The Lacteo lateral moraine 20 km up valley from the Rincon moraines
369 affords ages in range of 12.0 ± 0.4 ka to 14.6 ± 0.4 ka (Fig. 8). The ages
370 display a significant spread and a bi-modal distribution (Fig. 10 D). All
371 ages fall within 2σ of the weighted mean of 13.0 ± 1.0 ka, and thus there
372 is no statistical grounds for excluding any ages. However, the moraines are
373 morphostratigraphically younger than the Rincon moraines (12.9 ± 0.4 ka),
374 and so we exclude the older two ages (14.2 ± 0.6 and 14.6 ± 0.4 ka) as
375 outliers and instead use the weighted mean of the younger ages to date the
376 advance at 12.4 ± 0.3 ka. This interpretation fits with the wider chronology
377 throughout the valley. The two older samples were probably reworked from
378 an earlier advance.

379 Samples from a transect along the Río Lacteo valley (Fig. 8) yielded ages
380 of 24.1 ± 0.8 (RV1608), 10.1 ± 0.3 (RV1606), and 11.7 ± 0.6 ka (RV1609)
381 (in the order of distance from the Rincon moraines). The oldest sample
382 is chronostratigraphically an outlier and likely relates to the gLGM. The
383 remaining two ages likely afford minimum ages for deglaciation of the Lacteo
384 valley. The sample RV1609 came from a cobble on a bedrock outcrop about
385 30 m higher in elevation than the sample RV1606, which could explain its
386 older age despite being 4.5 km further up the valley.

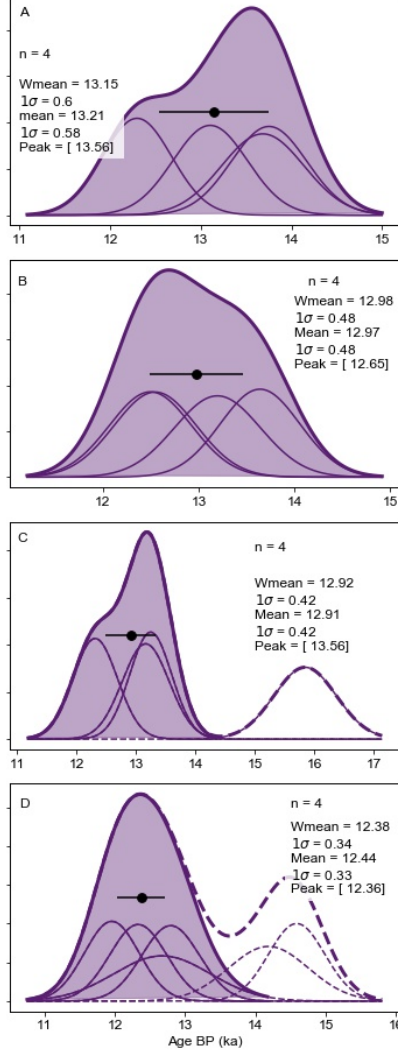


Figure 10: Normal kernel density diagrams for exposure ages from moraines: (A) the Belgrano inner moraines, (B) the Belgrano outer moraines, (C) the Rincon, and (D) the Lacteo lateral moraine. Thin purple curves represent Gaussian curves for each age and thick purple curves represent the summed probabilities. Outliers are represented by dashed lines. Circles represent uncertainties-weighted mean of ages after excluding the outliers, and 1 σ standard deviations.

387 4.2.3. *Palaeolake development*

388 The two ^{10}Be samples from the palaeo-shorelines yield ages of 12.4 ± 0.4
389 and 11.1 ± 0.4 ka, which is consistent with the slightly older ages for the
390 Belgrano moraines (Table 3 and Fig. 5). The age difference between the two
391 beach gravels could result from post-depositional processes or inheritance,
392 and without additional samples it is difficult to resolve. The OSL sample
393 (12.7 ± 0.7 ka) that came from glaciolacustrine sediments associated with
394 the 882 - 885 shoreline is within dating uncertainties consistent with the
395 shoreline ^{10}Be ages. The palaeolake likely formed at or before 12.7 ka and
396 persisted for at least several hundred years, but perhaps over a millennium.
397 The OSL sample from lacustrine sediments inboard of the Rincon moraines
398 (Fig. 5), with an age of 11.6 ± 1.1 ka, fits with the slightly older ^{10}Be ages
399 from the bounding Rincon moraines. This proglacial formed between the
400 Lacteo glacier and the Rincon moraines, and likely drained into palaeolake
401 Belgrano.

402 5. Discussion

403 5.1. *LGIT at Lago Belgrano*

404 Our ^{10}Be chronology indicates that a major re-advance of the Belgrano
405 and Lacteo glaciers culminated at ~ 13 ka toward the end of the ACR. At this
406 time, the Belgrano glacier advanced to within 8 km of its gLGM limit ($24.7 \pm$
407 1.0 ka, Mendelova et al., 2019). Our mapping reveals up to 10 advances/still-
408 stands during the ACR, but the dating resolution is insufficient to distinguish
409 between them. The reconstructed extent of the Belgrano and Lacteo glaciers
410 during the ACR is shown in Figure 11.

411 Following the culmination of these advances/still-stands, the ice margin
 412 retreated and abandoned the Belgrano moraines. In the process, a palaeolake
 413 formed at 882 - 885 m asl, which was dammed by ice at least 10 km west of
 414 the Belgrano moraines. The OSL age (12.7 ± 0.7 ka) from glaciolacustrine
 415 sediments and the ^{10}Be ages from lake shorelines (12.4 ± 0.4 and 11.1 ± 0.4
 416 ka) suggest that this lake formed at ~ 12.7 ka and likely existed throughout
 417 the YD period. A minimum radiocarbon age of 12.6 ± 0.06 cal ka BP (Wen-
 418 zens, 2005; Fig. 2) for ice retreat from the Belgrano moraines is consistent
 419 with this interpretation. Based on the above ages and the extent of mapped
 420 shorelines, we infer a retreat of at least 10 km within several hundred years,
 421 which was probably facilitated by calving in the proglacial lake. Although
 422 glacial retreat had initiated, the ice remained extensive enough to maintain
 423 an ice dam capable of blocking the southward drainage route through Lago
 424 Nansen.

425 The extent of mapped shorelines suggests that by this time, the Lacteo
 426 glacier had separated from the Belgrano glacier, and retreated at least 5 km
 427 from the Rincon moraines (Fig. 11). A proglacial lake formed inboard of
 428 the Rincon moraines. The OSL age from the glaciolacustrine sediments here
 429 (11.6 ± 1.1 ka) suggest that this lake existed at roughly the same time as the
 430 paleolake Belgrano. The lateral moraines further up the Lacteo valley, with
 431 an age of 12.4 ± 0.3 ka, indicates the glacier margin then stabilised during
 432 the YD. Two ages from bedrock outcrops in the Lacteo valley (10.1 ± 0.3
 433 and 11.7 ± 0.6 ka) indicate that the lower part of the valley deglaciated by
 434 the end of YD.

435 The moraines bounding Lago Burmeister occupy the same morphostrati-

436 graphic position as the Belgrano moraines, suggesting that they represent an
437 ACR advance of the Burmeister glacier. A minimum radiocarbon age from
438 a kettle within these moraines (Wenzens, 2005), however suggests that they
439 are mid-Holocene in age. Further chronological control would be needed to
440 confirm this.

441 *5.2. Deglaciation of the central sector of the PIS*

442 The PIS had retreated and thinned significantly during the first phase of
443 deglaciation after 18-19 ka (Boex et al., 2013; Hein et al., 2010; Henríquez
444 et al., 2017), and had started to separate into the Northern Patagonian Ice-
445 field and the San Lorenzo ice cap by ~ 15 ka (Davies et al., 2018; Thorndy-
446 craft et al., 2019). The major basins of Lago Puyeredón and Lago Buenos
447 Aires had deglaciated by about 16 ka (Hein et al., 2010; Turner et al., 2005;
448 Bendle et al., 2017; Boex et al., 2013). By the time of the ACR, ice margins
449 of the Northern Patagonian Icefield were within a few tens of km of the mod-
450 ern glacier margins (75-100 km upstream of the LGM limits; Davies et al.,
451 2018; Thorndycraft et al., 2019; Nimick et al., 2016). Northern and western
452 outlet glaciers of the San Lorenzo ice cap were no longer interacting with
453 the PIS, as evidenced by the ACR moraines deposited by the Tranquilo and
454 Calluqueo glaciers (Davies et al., 2018; Sagredo et al., 2018).

455 Our chronology from the Belgrano valley provides robust evidence for
456 glacier expansion in central Patagonia during the ACR. Cross-cutting of the
457 older Menelik moraines by the ACR Belgrano moraines demonstrates that
458 this was a re-advance, in the case of the Belgrano glacier, rather than a still-
459 stand during overall deglaciation. Together with the data from the Salto and
460 Tranquilo valleys (Davies et al., 2018; Sagredo et al., 2018), this indicates

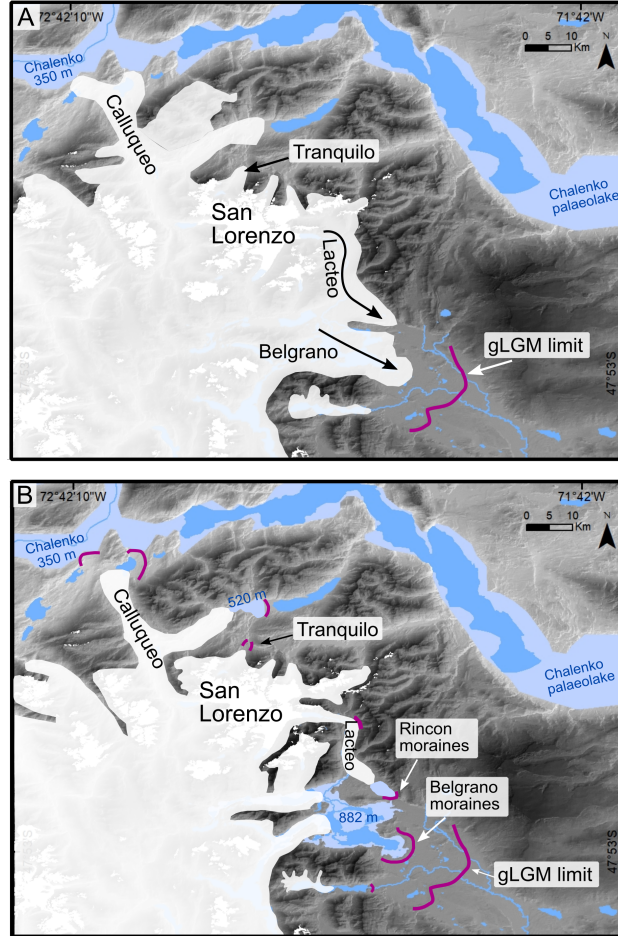


Figure 11: Model of ice and palaeolake evolution (A) during the ACR and (B) during the YD. The extent of the Belgrano and Lacteo glaciers during the ACR, and the extent of the palaeolake Belgrano during the YD are based on our geomorphological mapping and chronology. The extent of the Calluqueo and Tranquilo glaciers, and palaeolakes (pale blue) on the northern flanks of the San Lorenzo is based on published work (Davies et al., 2018; Sagredo et al., 2018; Glasser et al., 2012; Martin et al., 2019; Thorndycraft et al., 2019). Moraines delineating the extent of these glaciers are highlighted in pink. Elevation of the palaeolakes is also indicated in m asl. Darker blue colour indicates modern lakes.

461 a uniform response of the San Lorenzo glaciers to the ACR climate signal.
462 To maintain an outlet glacier in the Belgrano valley, the ice cap likely also
463 covered mountains to the south of the San Lorenzo massif, but the wider
464 geomorphology suggest it was largely independent of the shrinking ice-sheet
465 by this time.

466 Glacier advances/still-stands in central Patagonia during the ACR were
467 a response to colder and wetter conditions reconstructed from pollen data.
468 The Lago Edita record (47° S, Henríquez et al., 2017) revealed an increase
469 in cold-resistant taxa between 14 ka - 13.5 ka. A northward expansion of
470 the Magellanic moorland between 14.5 - 12.8 ka was documented by a ma-
471 rine pollen record off the Chilean coast (46° S, Montade et al., 2013; Fig.
472 12). These palaeovegetation changes were interpreted to indicate increased
473 precipitation due to enhanced influence of the SWW at this latitude, and
474 a pause in deglacial warming in the area (Henríquez et al., 2017; Montade
475 et al., 2013).

476 Following the ACR advances, ice in the Belgrano valley retreated by at
477 least 10 km before stabilising again. This is evidenced by the palaeolake Bel-
478 grano, which formed once ice abandoned the Belgrano moraines and existed
479 during the YD period, as well as by the lateral moraines in the Lacteo valley
480 (12.4 ± 0.3 ka). The initial ice recession was likely a response to regional
481 warming trend as indicated by the retreat of the Magellanic moorland after
482 12.8 ka (Montade et al., 2013; Fig. 12), and palaeovegetation changes in the
483 Lago Edita record (Henríquez et al., 2017). The YD ice margin stabilisation
484 in central Patagonia is supported by provisional ^{10}Be ages from moraines
485 inboard of the ACR limits in the Tranquilo and Salto valleys (Fig. 2; Glasser

et al., 2012; Sagredo et al., 2018), and by ^{10}Be ages from the eastern side of the Northern Patagonian Icefield (Nimick et al., 2016; Glasser et al., 2012). Minor advances or still stands during the YD may reflect the continued influence of the SWW in central Patagonia. Pollen assemblages from the Lago Augusta core (47°S) were interpreted to indicate a highly variable precipitation regime under cool/wet climate between 13.8 and 11.8 ka (Villa-Martínez et al., 2012), while palaeovegetation changes in the Lago Edita record were interpreted to reflect the declining but continued influence of the SWW under warmer conditions until 11 ka (Henríquez et al., 2017).

Our data provide support for the final break-up and a complete separation of the PIS into the Northern Patagonian Icefield, the San Lorenzo and the Southern Patagonian Icefield by the end of the YD, when the ice-dammed palaeolake Belgrano drained. Our exposure ages from the palaeoshorelines (12.4 ± 0.4 , 11.1 ± 0.4 ka) indicate that the Belgrano palaeolake likely drained at similar time as the palaeolake Chalenko (Fig. 11 with a Bayesian modelled age of 12 - 11 ka (Thorndycraft et al., 2019). By this time ice masses in central Patagonia were likely close to their present day configuration.

5.3. *Factors controlling the relative magnitude of glacier advances*

The ACR re-advance of the Belgrano glacier reached to within 8 km of its gLGM extent. This is in contrast with the ACR ice margins east of the Northern Patagonian Icefield and on the northern flank of San Lorenzo, which are $\sim 100 - 120$ km upvalley from the gLGM limits. While the Belgrano ACR advance was primarily climatically controlled, the relative magnitude of the ACR and gLGM advances at Lago Belgrano can, at least in part, be explained by ice divide migration, catchment size and ice flow re-routing.

511 During the gLGM, the ice divide of the PIS was located west of San
512 Lorenzo, along the main chain of the Andes. This potentially reduced the
513 catchment size of the Belgrano glacier due to ice flow re-routing, while ice
514 from the northern side of San Lorenzo was confluent with ice from the North-
515 ern Patagonian icefield and focused ice flow into the Lago Pueyrredón valley.
516 This allowed a glacier in the Lago Pueyrredón valley to advance further east,
517 while the Belgrano glacier was relatively small at the gLGM. The full eleva-
518 tion of the PIS also blocked westerly moisture penetration (Mendelova et al.,
519 2019) and reduced snow fall over San Lorenzo during the gLGM further
520 restricting the Belgrano glacier.

521 During deglaciation, the ice divide would have migrated eastward as the
522 PIS thinned and broke down along its major basins, leading to ice flow reor-
523 ganization and eventual ice divide break-up prior to the ACR. Glacier in the
524 Lago Pueyrredón valley would have largely disintegrated by this time leaving
525 ice margins of the former tributaries 100 - 120 km upstream of the gLGM
526 limit (Hein et al., 2010; Turner et al., 2005; Boex et al., 2013; Henríquez et al.,
527 2017). The thinning PIS would have also allowed for increased penetration of
528 westerly precipitation to the San Lorenzo massif, relative to the gLGM, and
529 enabled the Belgrano glacier to advance close to its gLGM limit. This pro-
530 cess also explains why the Belgrano glacier was considerably smaller during
531 the gLGM compared to its maximum extent of the last glacial cycle at ~ 75
532 ka (Mendelova et al., 2019). Thus, the real anomaly in the Belgrano valley is
533 the comparatively small gLGM ice extent, rather than an exceptionally large
534 ACR.

535 The catchment size and hypsometry also played a role in determining rel-

536 ative extents of the San Lorenzo glaciers during the ACR. The small extent
 537 of the Tranquilo glacier during the ACR, compared to the Belgrano and Cal-
 538 luqueo glaciers can be explained by their catchment size. While the former
 539 had a single smaller accumulation area on San Lorenzo (Sagredo et al., 2018),
 540 the latter two had additional ice contribution from the surrounding moun-
 541 tains. The difference in hypsometry will have played a role. The northern
 542 and western flanks of San Lorenzo have greater relief and a steeper elevation
 543 profile, and thus glaciers here would reach the ablation zone in a shorter
 544 distance when compared to ice discharging into the high elevation Belgrano
 545 valley to the east. A somewhat lower ELA on the western side of San Lorenzo
 546 (Falaschi et al., 2013), would have, to some extent, compensated for the lower
 547 altitude of the Salto valley and thereby allow the Calluqueo glacier to advance
 548 to the lower elevation of ~ 300 m asl (Davies et al., 2018).

549 *5.4. Regional view*

550 Our data reveals a structure of the LGIT advances/still-stands at Lago
 551 Belgrano that is similar to southern Patagonia (51° S - 50° S; García et al.,
 552 2012; Moreno et al., 2009; Fogwill and Kubik, 2005; Ackert et al., 2008; Strelin
 553 et al., 2011; Kaplan et al., 2011) and New Zealand (Putnam et al., 2010a;
 554 Kaplan et al., 2010, 2013). Glaciers were most extensive during the ACR
 555 and then underwent recession punctuated by smaller advances/still-stands
 556 during the YD.

557 The ACR cooling is recorded in pollen records from NW Patagonia (41°
 558 - 43° S; Moreno and Videla, 2016; Pesce and Moreno, 2014), and a pause in
 559 deglacial warming coeval with the ACR is reflected in sea surface tempera-
 560 ture records along the Chilean coast as far north as 41° S (Fig. 12; Kaiser

et al., 2005; Haddam et al., 2018; Caniupán et al., 2011). At the moment, there are no glacial chronologies spanning the LGIT in northern Patagonia to evaluate the glacier response to cold reversals here. In southernmost Patagonia (54° S - 55° S), contradictory interpretations of the ACR extent of the Cordillera Darwin ice field warrant further work (McCulloch et al., 2005; Hall et al., 2013, 2017). East of the Cordillera Darwin, glaciers were confined to cirques during the ACR (Menounos et al., 2013). Colder climatic conditions during the ACR in Tierra del Fuego (53° S) are, however, indicated by palaeovegetation proxies (Mansilla et al., 2016).

Our data supports a widespread atmospheric and oceanic cooling throughout the southern mid-latitudes contemporaneous with cooling identified in the Antarctic ice cores (Fig. 12). Latitudinal displacement of the SWW belt and associated oceanic fronts could facilitate the propagation of the climate signals (Pesce and Moreno, 2014; Moreno et al., 2012; Lamy, 2004). A northward shift of the coupled system during the ACR would have caused cooling and increased precipitation, promoting glacier expansion in Patagonia and New Zealand (García et al., 2012; Sagredo et al., 2018; Putnam et al., 2010b). Such a shift in the coupled system was likely driven by interhemispheric oceanic teleconnections and associated atmospheric reorganization commonly attributed to the bipolar see-saw (Pedro et al., 2018; Stocker and Johnsen, 2003; Buizert et al., 2018).

6. Conclusions

Our geomorphological mapping along with ^{10}Be and OSL ages document a major re-advance of the Belgrano glacier at 13.1 ± 0.6 ka, and a

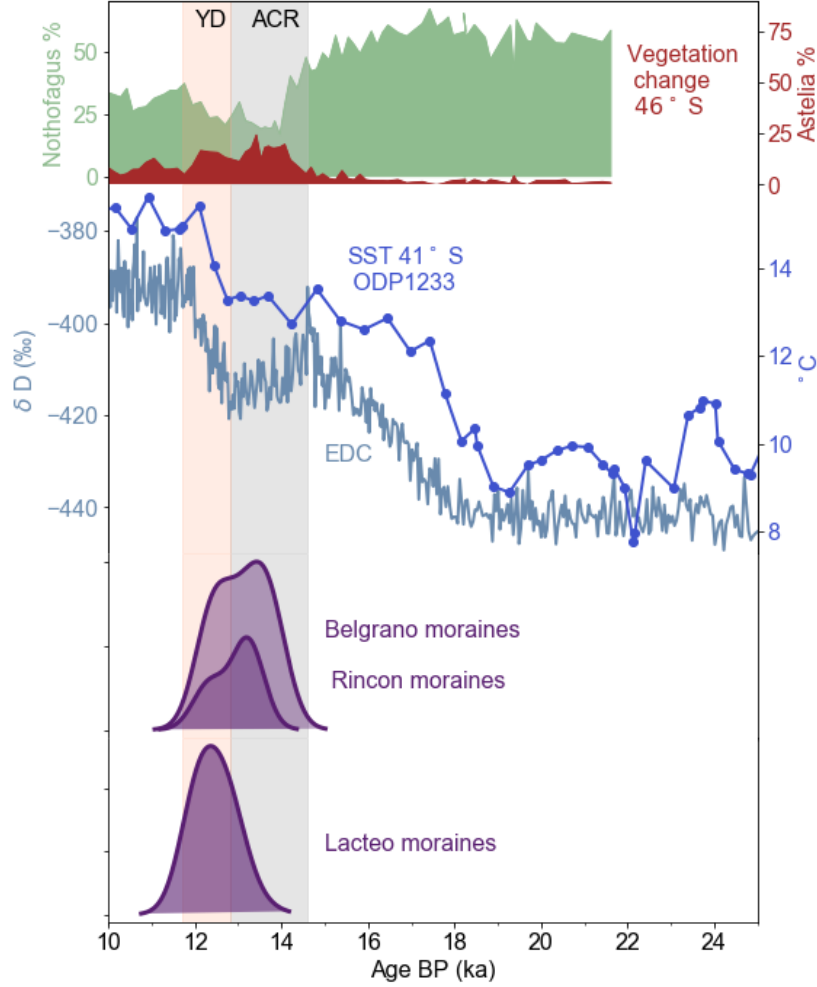


Figure 12: Comparison of our exposure ages to other proxies: *Nothofagus dombeyi* type and *Astelia pumila* pollen record from core MD07-3088 off the Chilean coast (46° S, Montade et al., 2013) plotted on a scale from Montade et al. (2019), sea surface temperature reconstruction from core ODP 1233 off the Chilean coast (Kaiser et al., 2005) and the δD record from EDC, east Antarctica (EPICA Community Members, 2004) plotted on AICC2012 timescale (Veres et al., 2013). The exposure ages are plotted after outliers have been removed. *Astelia* is a plant typical of the Magellanic moorland that at present grows south of 48° S.

re-advance/still-stand of the Lacteo glacier at 12.9 ± 0.4 ka, coeval with the ACR. The San Lorenzo ice cap covered an extensive area at this time, but was largely independent of at least the Northern Patagonian Icefield. Following the culmination of the ACR advances/still-stands, ice in the Belgrano valley retreated by at least 10 km and an ice-dammed proglacial lake formed at 882 - 885 m asl. The ^{10}Be ages from the palaeoshorelines and an OSL age from glaciolacustrine sediments suggest that the lake likely existed between ~ 12.7 and ~ 11.1 ka, implying stabilisation of ice margins during the YD. The ^{10}Be ages from a lateral moraine in the Lacteo valley (12.4 ± 0.3 ka) indicate a smaller advance/still-stand during the YD. We suggest that the final break-up of the PIS occurred at the end of the YD, when glaciers retreated back to the mountains and the palaeolake Belgrano drained. Our data from the Belgrano valley supports the dominant ACR climate signal in the southern mid-latitudes, but also suggest a co-occurrence of the northern hemisphere YD signal, albeit of smaller magnitude. Glacier expansion in the southern mid-latitudes during the ACR is in line with the northward migration of the coupled oceanic-atmospheric system.

Acknowledgements

This work was supported by a NERC PhD studentship (NE/L002558/1) to MM and a NERC CIAF grant (CIAF.9167.0416). We also acknowledge funding from the British Society for Geomorphology, Quaternary Research Association, Royal Geographical Society (with IBG), the Explorers Club, the Scottish Alliance for Geoscience, Environment and Society (Small Grants Scheme), and the Moray Endowment Fund from the University of Edinburgh.

609 We are grateful to Andrew Gray for his help with fieldwork and Patricio
610 Parada for arranging export of samples. The national park authorities of
611 Argentina are thanked for granting permission to conduct fieldwork, and the
612 rangers of the Perito Moreno National Park are thanked in particular for
613 their assistance in the field. Jenny Bradley is thanked for preparing the
614 samples for OSL dating at the University of Liverpool. We would like to
615 thank D.Sugden and R.McCulloch for insightful discussions. Bethan Davies
616 and Mike Bentley are thanked for their constructive comments that greatly
617 improved this manuscript.

618 **Supplementary Information**

619 *OSL methods*

620 Samples for luminescence dating were collected in opaque tubes and pre-
621 pared for analysis under subdued lighting conditions. To calculate the envi-
622 ronmental dose-rate throughout burial for each sample, U, Th and K concen-
623 trations were measured for ~ 80 g of the bulk sediment sample using high-
624 resolution gamma spectrometry. Water contents of 5 ± 2 % were estimated
625 considering the field water contents, and the environmental history for each
626 sample. Cosmic dose-rates were calculated after Prescott and Hutton (1994).
627 Environmental dose-rates determined for samples RV1801 and LBSH1801 are
628 shown in Table S1. Grains of K-feldspar were used to determine equivalent
629 doses (D_e). Samples were first treated with a 10 % v/v dilution of 37 % HCl
630 and with 20 % v/v of H_2O_2 to remove carbonates and organics, respectively.
631 Dry sieving then isolated the 125 - 180 μm (sample LBSH1801) or 212 - 250
632 μm (sample RV1801) diameter grains, which were subject to density sepa-

633 ration using sodium polytungstate ($< 2.58 \text{ g cm}^{-3}$ K-feldspar dominated)
 634 and then not etched using hydrofluoric acid. Finally, grains of K-feldspar
 635 were mounted on a 9.8 mm diameter aluminium single-grain disc for anal-
 636 ysis, which contained a 10 by 10 grid of $300 \mu\text{m}$ diameter holes. Note that
 637 sample LBSH01-01 was analysed using microhole analysis rather than single
 638 grains (i.e. up to four grains in each hole due to a grain size of 125 - 180
 639 μm). All luminescence measurements were performed using a RisøTL/OSL
 640 DA-15 automated single-grain system equipped with a $^{90}\text{Sr}/^{90}\text{Y}$ beta source
 641 (Bøtter-Jensen et al., 2003) fitted with a blue filter pack (BG39, Corning 7-59)
 642 in front of the photomultiplier tube. Single aliquot regenerative dose (SAR)
 643 protocols (Murray and Wintle, 2000) were used for the post-IR IRSL analy-
 644 ses performed at 225°C (Thomsen et al., 2008), termed the pIRIR₂₂₅ signal.
 645 A preheat temperature of 250°C for 60 s was used prior to stimulations of 2
 646 s using the infra-red laser at 225°C . The IRSL signal measured performed
 647 at 50°C prior to the pIRIR₂₂₅ measurement and the elevated temperature
 648 bleach of 330°C for 200 s at the end of each L_x/T_x cycle were performed
 649 using the IR LEDs. The location of the single-grain discs was performed
 650 at room temperature, rather than elevated temperatures to prevent thermal
 651 annealing of the IRSL signal (after Smedley and Duller, 2013). The first 0.3 s
 652 and final 0.6 s of stimulation were summed to calculate the initial and back-
 653 ground IRSL signals, respectively. The grains were accepted after applying
 654 the following screening criteria and accounting for the associated uncertain-
 655 ties: (1) whether the test dose response was greater than three sigma above
 656 the background, (2) whether the test dose uncertainty was less than 10 %,
 657 (3) whether the recycling and OSL-IR depletion ratios were within the range

658 of ratios 0.9 to 1.1, and (4) whether recuperation was less than 5 % of the
 659 response from the largest regenerative dose. Grains from both samples were
 660 used for dose-recovery experiments and successfully recovered a given dose
 661 within 10 % using the pIRIR₂₂₅ signal. Fading experiments were performed
 662 on three multi-grain aliquots per sample and reported g-values of -0.4 ± 0.7
 663 %/decade (RV18-01) and -1.0 ± 0.7 %/decade (LBSH18-01), which suggests
 664 that no fading correction was required for the pIRIR₂₂₅ signal. D_e values were
 665 calculated from all grains passing all the screening criteria. The minimum
 666 age model (MAM; (Galbraith et al., 1999; Galbraith and Laslett, 1993)) was
 667 applied to determine an age for the samples as the asymmetrical D_e distribu-
 668 tions suggested the samples were partially bleached prior to burial (Fig. S1).
 669 The scatter in the D_e distribution arising from intrinsic and extrinsic sources
 670 were combined in quadrature to determine σ_b for the MAM (Table S1). The
 671 overdispersion values arising from intrinsic sources for sample RV1801 (12
 672 %) and LBSH18-01 (13 %) were derived from the dose-recovery experiments,
 673 while the over-dispersion arising from variability in the internal dose-rates of
 674 K-feldspar grains for both samples was assumed to be 10 % (after Smedley
 675 and Pearce, 2016). Additional over-dispersion (20 %) was incorporated for
 676 sample RV1801 to account for the variability in single-grain D_e distributions
 677 caused by external microdosimetry (after Smedley et al. 2017). The D_e val-
 678 ues were then divided by the environmental dose-rates to determine an age
 679 for each sample (Table S1).

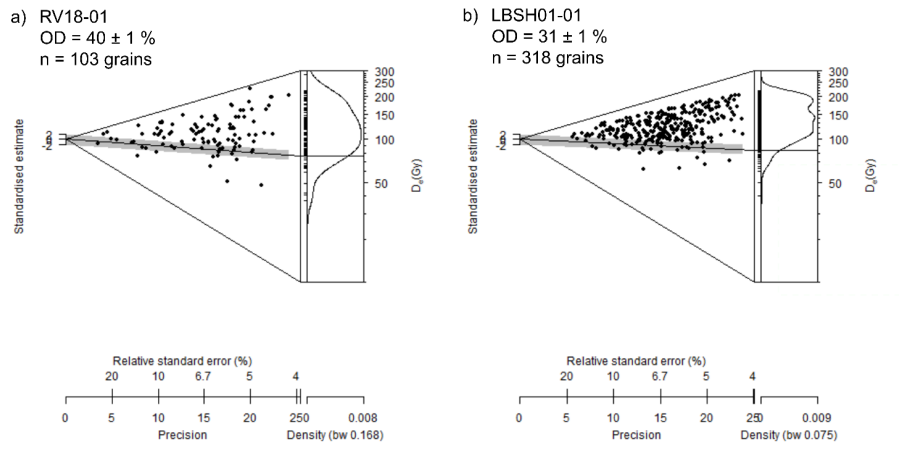


Figure 1: Abanico plots of the D_e values determined for OSL dating, where the grey shading shows the MAM D_e for each distribution. Note that sample LBSH0101 was analysed using microhole analysis rather than single grains (i.e. up to four grains in each hole due to a grain size of 125–180 μm) but it is likely that the OSL signal was dominated by one brighter grain.

References

- Ackert, R., Becker, R.A., Singer, B.S., Kurz, M.D., Caffee, M.W., Mickelson, D.M., 2008. Patgonian Glacier Response during the Late Glacial Holocene Transition. *Science* 321, 392–396.
- Anderson, R.F., Ali, S., Bradtmiller, L.I., Nielsen, S.H.H., Fleisher, M.Q., Anderson, B.E., Burckle, L.H., 2009. Wind-Driven Upwelling in the Southern Ocean and the Deglacial Rise in Atmospheric CO₂. *Science* 323, 1443–1448.
- Balco, G., Stone, J.O., Lifton, N.A., Dunai, T.J., 2008. A complete and easily accessible means of calculating surface exposure ages or erosion rates from ¹⁰Be and ²⁶Al measurements. *Quaternary Geochronology* 3, 174–195.
- Bendle, J.M., Thorndycraft, V.R., Palmer, A.P., 2017. The glacial geomorphology of the Lago Buenos Aires and Lago Pueyrredón ice lobes of central Patagonia. *Journal of Maps* 13, 654–673.
- Bennett, K.D., 2000. The Last Glacial-Holocene Transition in Southern Chile. *Science* 290, 325–328.
- Björck, S., Rundgren, M., Ljung, K., Unkel, I., Wallin, ., 2012. Multi-proxy analyses of a peat bog on Isla de los Estados, easternmost Tierra del Fuego: A unique record of the variable Southern Hemisphere Westerlies since the last deglaciation. *Quaternary Science Reviews* 42, 1–14.
- Blunier, T., Chappellaz, J., Schwander, J., Dällenbach, A., Stauffer, B., Stocker, T.F., Raynaud, D., Jouzel, J., Clausen, H.B., Hammer, C.U.,

- Johnsen, S.J., 1998. Asynchrony of Antarctic and Greenland climate change during the last glacial period. *Nature* 394, 739–743.
- Boex, J., Fogwill, C., Harrison, S., Glasser, N.F., Hein, A., Schnabel, C., Xu, S., 2013. Rapid thinning of the late Pleistocene Patagonian Ice Sheet followed migration of the Southern Westerlies. *Scientific Reports* 3, 2118.
- Borchers, B., Marrero, S., Balco, G., Caffee, M., Goehring, B., Lifton, N., Nishiizumi, K., Phillips, F., Schaefer, J., Stone, J., 2016. Geological calibration of spallation production rates in the CRONUS-Earth project. *Quaternary Geochronology* 31, 188–198.
- Bøtter-Jensen, L., Andersen, C., Duller, G., Murray, A., 2003. Developments in radiation, stimulation and observation facilities in luminescence measurements. *Radiation Measurements* 37, 535–541.
- Bronk Ramsey, C., 2009. Bayesian Analysis of Radiocarbon Dates. *Radiocarbon* 51, 337–360.
- Buizert, C., Sigl, M., Severi, M., Markle, B.R., Wettstein, J.J., McConnell, J.R., Pedro, J.B., Sodemann, H., Goto-Azuma, K., Kawamura, K., Fujita, S., Motoyama, H., Hirabayashi, M., Uemura, R., Stenni, B., Parrenin, F., He, F., Fudge, T.J., Steig, E.J., 2018. Abrupt ice-age shifts in southern westerly winds and Antarctic climate forced from the north. *Nature* 563, 681–685.
- Caldenius, C., 1932. Las glaciaciones cuaternarias en la Patagonia y Tierra del Fuego. *Geografiska Annaler* 14, 1–164.

- Caniupán, M., Lamy, F., Lange, C.B., Kaiser, J., Arz, H., Kilian, R., Baeza Urrea, O., Aracena, C., Hebbeln, D., Kissel, C., Laj, C., Mollenhauer, G., Tiedemann, R., 2011. Millennial-scale sea surface temperature and Patagonian Ice Sheet changes off southernmost Chile (53 °S) over the past 60 kyr. *Paleoceanography* 26, 1–10.
- Darvill, C.M., 2013. Cosmogenic nuclide analysis. *Geomorphological techniques* 10, 1–25.
- Darvill, C.M., Stokes, C.R., Bentley, M.J., Lovell, H., 2014. A glacial geomorphological map of the southernmost ice lobes of Patagonia: the Bahía Inútil San Sebastián, Magellan, Otway, Skyring and Río Gallegos lobes. *Journal of Maps* 10, 500–520.
- Davies, B., Thorndycraft, V., Fabel, D., Martin, J., 2018. Asynchronous glacier dynamics during the Antarctic Cold Reversal in central Patagonia. *Quaternary Science Reviews* 200, 287–312.
- De Angelis, H., Miles, E., Moelg, N., Paul, F., Sharp, M., Wyatt, F., 2015. GLIMS Glacier Database.
- De Arellano, C.R., Putlitz, B., Müntener, O., Ovtcharova, M., 2012. High precision U/Pb zircon dating of the Chaltén Plutonic Complex (Cerro Fitz Roy, Patagonia) and its relationship to arc migration in the southernmost Andes. *Tectonics* 31.
- Denton, G., Heusser, C.J., Lowel, T., Moreno, P., Andersen, B., Heusser, L.E., Schluhter, C., Marchant, D., 1999. Interhemispheric Linkage of Pa-

- leoclimate During the Last Glaciation. *Geografiska Annaler, Series A: Physical Geography* 81, 107–153.
- Denton, G.H., Anderson, R.F., Toggweiler, J.R., Edwards, R.L., Schaefer, J.M., Putnam, a.E., 2010. The Last Glacial Termination. *Science* 328, 1652–1656.
- Douglass, D.C., Singer, B.S., Ackert, R.P., Kaplan, M.R., Caffee, M.W., 2007. Constraining Boulder Erosion Rates and Ages of Mid-Pleistocene Moraines. Lago Buenos Aires, Argentina. *GSA Abstracts and Programs Northeastern Section, 42nd Annual Meeting* .
- EPICA Community Members, 2004. Eight glacial cycles from an Antarctic ice core. *Nature* 429, 623–628.
- Falaschi, D., Bolch, T., Rastner, P., Lenzano, M.G., Lenzano, L., Lo Vecchio, A., Moragues, S., 2017. Mass changes of alpine glaciers at the eastern margin of the Northern and Southern Patagonian Icefields between 2000 and 2012. *Journal of Glaciology* 63, 258–272.
- Falaschi, D., Bravo, C., Masiokas, M., Villalba, R., Rivera, A., 2013. First Glacier Inventory and Recent Changes in Glacier Area in the Monte San Lorenzo Region (47°S), Southern Patagonian Andes, South America. *Arctic, Antarctic, and Alpine Research* 45, 19–28.
- Fogwill, C.J., Kubik, P.W., 2005. A glacial stage spanning the Antarctic Cold Reversal in Torres del Paine (51°S), Chile, based on preliminary cosmogenic exposure ages. *Geografiska Annaler, Series A: Physical Geography* 87, 403–408.

- Galbraith, R., Laslett, G., 1993. Statistical models for mixed fission track ages. *Nuclear Tracks and Radiation Measurements* 21, 459–470.
- Galbraith, R.F., Roberts, R.G., Laslett, G.M., Yoshida, H., Olley, J.M., 1999. Optical dating of single and multiple grains of quartz from Jinnium rock shelter, northern Australia: Part I, experimental design and statistical models. *Archaeometry* 41, 339–364.
- García, J.L., Kaplan, M.R., Hall, B.L., Schaefer, J.M., Vega, R.M., Schwartz, R., Finkel, R., 2012. Glacier expansion in southern Patagonia throughout the Antarctic cold reversal. *Geology* 40, 859–862.
- Garibotti, I.A., Villalba, R., 2017. Colonization of mid- and late-Holocene moraines by lichens and trees in the Magellanic sub-Antarctic province. *Polar Biology* 40, 1739–1753.
- Garreaud, R., Lopez, P., Minvielle, M., Rojas, M., 2013. Large-scale control on the Patagonian climate. *Journal of Climate* 26, 215–230.
- Glasser, N.F., Harrison, S., Schnabel, C., Fabel, D., Jansson, K.N., 2012. Younger Dryas and early Holocene age glacier advances in Patagonia. *Quaternary Science Reviews* 58, 7–17.
- Glasser, N.F., Jansson, K.N., Harrison, S., Kleman, J., 2008. The glacial geomorphology and Pleistocene history of South America between 38°S and 56°S. *Quaternary Science Reviews* 27, 365–390.
- Glasser, N.F., Jansson, K.N., Harrison, S., Rivera, A., 2005. Geomorphological evidence for variations of the North Patagonian Icefield during the Holocene. *Geomorphology* 71, 263–277.

- Gosse, J.C., Phillips, F.M., 2001. Terrestrial in situ cosmogenic nuclides: Theory and application. *Quaternary Science Reviews* 20, 1475–1560.
- Haberle, S.G., Bennett, K.D., 2004. Postglacial formation and dynamics of North Patagonian Rainforest in the Chonos Archipelago, Southern Chile. *Quaternary Science Reviews* 23, 2433–2452.
- Haddam, N.A., Siani, G., Michel, E., Kaiser, J., Lamy, F., Duchamp-Alphonse, S., Hefter, J., Braconnot, P., Dewilde, F., Isgüder, G., Tisnerat-Laborde, N., Thil, F., Durand, N., Kissel, C., 2018. Changes in latitudinal sea surface temperature gradients along the Southern Chilean margin since the last glacial. *Quaternary Science Reviews* 194, 62–76.
- Hall, B.L., Denton, G., Lowell, T., Bromley, G.R.M., Putnam, A.E., 2017. Retreat of the Cordillera Darwin icefield during Termination I. *Cuadernos de Investigación Geográfica* 0.
- Hall, B.L., Porter, C.T., Denton, G.H., Lowell, T.V., Bromley, G.R.M., 2013. Extensive recession of Cordillera Darwin glaciers in southernmost South America during Heinrich Stadial 1. *Quaternary Science Reviews* 62, 49–55.
- Hein, A.S., Coge, A., Darvill, C.M., Mendelova, M., Kaplan, M.R., Herman, F., Dunai, T.J., Norton, K., Xu, S., Christl, M., Rodés, ., 2017. Regional mid-Pleistocene glaciation in central Patagonia. *Quaternary Science Reviews* 164, 77–94.
- Hein, A.S., Hulton, N.R., Dunai, T.J., Sugden, D.E., Kaplan, M.R., Xu, S., 2010. The chronology of the Last Glacial Maximum and deglacial events in central Argentine Patagonia. *Quaternary Science Reviews* 29, 1212–1227.

- Henríquez, W.I., Villa-Martínez, R., Vilanova, I., De Pol-Holz, R., Moreno, P.I., 2017. The last glacial termination on the eastern flank of the central Patagonian Andes (47 ° S). *Climate of the Past* 13, 879–895.
- Hogg, A.G., Hua, Q., Blackwell, P.G., Niu, M., Buck, C.E., Guilderson, T.P., Heaton, T.J., Palmer, J.G., Reimer, P.J., Reimer, R.W., Turney, C.S.M., Zimmerman, S.R.H., 2013. SHCal13 Southern Hemisphere Calibration, 050,000 Years cal BP. *Radiocarbon* 55, 1889–1903.
- Horta, L.R., Georgieff, S.M., Aschero, C.A., Goñi, R.A., 2017. Paleolacustrine records from Late Pleistocene–Holocene in the Perito Moreno National Park, Argentinian Patagonian Andes. *Quaternary International* 436, 8–15.
- Iglesias, V., Markgraf, V., Whitlock, C., 2016. 17,000 years of vegetation, fire and climate change in the eastern foothills of the Andes (lat. 44°S). *Palaeogeography, Palaeoclimatology, Palaeoecology* 457, 195–208.
- Kaiser, J., Lamy, F., Hebbeln, D., 2005. A 70-kyr sea surface temperature record off southern Chile (Ocean Drilling Program Site 1233). *Paleoceanography* 20, PA4009.
- Kaplan, M.R., Schaefer, J.M., Denton, G.H., Barrell, D.J.A., Chinn, T.J.H., Putnam, A.E., Andersen, B.G., Finkel, R.C., Schwartz, R., Doughty, A.M., 2010. Glacier retreat in New Zealand during the Younger Dryas stadial. *Nature* 467, 194–197.
- Kaplan, M.R., Schaefer, J.M., Denton, G.H., Doughty, A.M., Barrell, D.J.A., Chinn, T.J.H., Putnam, A.E., Andersen, B.G., Mackintosh, A., Finkel,

- R.C., Schwartz, R., Anderson, B., 2013. The anatomy of long-term warming since 15 ka in New Zealand based on net glacier snowline rise. *Geology* 41, 887–890.
- Kaplan, M.R., Strelin, J.A., Schaefer, J.M., Denton, G.H., Finkel, R.C., Schwartz, R., Putnam, A.E., Vandergoes, M.J., Goehring, B.M., Travis, S.G., 2011. In-situ cosmogenic ^{10}Be production rate at Lago Argentino, Patagonia: Implications for late-glacial climate chronology. *Earth and Planetary Science Letters* 309, 21–32.
- Lal, D., 1991. Cosmic ray labeling of erosion surfaces: in situ nuclide production rates and erosion models. *Earth and Planetary Science Letters* 104, 424–439.
- Lamy, F., 2004. Antarctic Timing of Surface Water Changes off Chile and Patagonian Ice Sheet Response. *Science* 304, 1959–1962.
- Lamy, F., Kaiser, J., Arz, H.W., Hebbeln, D., Ninnemann, U., Timm, O., Timmermann, A., Toggweiler, J., 2007. Modulation of the bipolar seesaw in the Southeast Pacific during Termination 1. *Earth and Planetary Science Letters* 259, 400–413.
- Lemieux-Dudon, B., Blayo, E., Petit, J.R., Waelbroeck, C., Svensson, A., Ritz, C., Barnola, J.M., Narcisi, B.M., Parrenin, F., 2010. Consistent dating for Antarctic and Greenland ice cores. *Quaternary Science Reviews* 29, 8–20.
- Lumley, S., Switsur, R., 1993. Late Quaternary Chronology of the Taitao peninsula, southern Chile. *Journal of Quaternary Science* 8, 161–165.

- Mansilla, C.A., McCulloch, R.D., Morello, F., 2016. Palaeoenvironmental change in Southern Patagonia during the Lateglacial and Holocene: Implications for forest refugia and climate reconstructions. *Palaeogeography, Palaeoclimatology, Palaeoecology* 447, 1–11.
- Markgraf, V., Whitlock, C., Haberle, S., 2007. Vegetation and fire history during the last 18,000 cal yr B.P. in Southern Patagonia: Mallín Pol-lux, Coyhaique, Province Aisén (45°41'30" S, 71°50'30" W, 640 m elevation). *Palaeogeography, Palaeoclimatology, Palaeoecology* 254, 492–507.
- Marshall, J., Speer, K., 2012. Closure of the meridional overturning circulation through Southern Ocean upwelling. *Nature Geoscience* 5, 171–180.
- Martin, J.R., Davies, B.J., Thorndycraft, V.R., 2019. Glacier dynamics during a phase of Late Quaternary warming in Patagonia reconstructed from sediment-landform associations. *Geomorphology* 337, 111–133.
- McCulloch, R., Bentley, M., Tipping, R., Clapperton, C., 2005. Evidence for LateGlacial Ice Dammed Lakes In The Central Strait Of Magellan And Bahía Inútil, Southernmost South America. *Geografiska Annaler, Series A: Physical Geography* 87, 335–362.
- Meijers, A.J., 2014. The Southern Ocean in the Coupled Model Intercomparison Project phase 5. *Philosophical Transactions of the Royal Society A: Mathematical, Physical and Engineering Sciences* 372.
- Mendelova, M., Hein, A., McCulloch, R., Davies, B., 2017. The Last Glacial Maximum and deglaciation in central Patagonia, 44°S–49°S. *Cuadernos de Investigación Geográfica* 43, 719.

- Mendelova, M., Hein, A.S., Rodes, A., Xu, S., 2019. Extensive mountain glaciation in central Patagonia during Marine Isotope Stage 5. *Quaternary Science Reviews* (Accepted).
- Menounos, B., Clague, J.J., Osborn, G., Davis, P.T., Ponce, F., Goehring, B.M., Maurer, M., Rabassa, J.O., Coronato, A., Marr, R., 2013. Latest Pleistocene and Holocene glacier fluctuations in southernmost Tierra del Fuego, Argentina. *Quaternary Science Reviews* 77, 70–79.
- Mercer, J.H., 1984. Simultaneous climatic change in both hemispheres and similar bipolar interglacial warming: Evidence and implications, in: Hansen, J.E., Takahashi, T. (Eds.), *Climate Processes and Climate Sensitivity*. American Geophysical Union, Washington, D. C.. volume 29 of *Geophysical Monograph Series*, pp. 307–313.
- Montade, V., Combourieu Nebout, N., Kissel, C., Haberle, S.G., Siani, G., Michel, E., 2013. Vegetation and climate changes during the last 22,000yr from a marine core near Taitao Peninsula, southern Chile. *Palaeogeography, Palaeoclimatology, Palaeoecology* 369, 335–348.
- Montade, V., Peyron, O., Favier, C., Francois, J.P., Haberle, S.G., 2019. A pollen-climate calibration from western Patagonia for palaeoclimatic reconstructions. *Journal of Quaternary Science* 34, 76–86.
- Moreno, P.I., Kaplan, M.R., François, J.P., Villa-Martínez, R., Moy, C.M., Stern, C.R., Kubik, P.W., 2009. Renewed glacial activity during the Antarctic cold reversal and persistence of cold conditions until 11.5 ka in southwestern Patagonia. *Geology* 37, 375–378.

- Moreno, P.I., Videla, J., 2016. Centennial and millennial-scale hydroclimate changes in northwestern Patagonia since 16,000 yr BP. *Quaternary Science Reviews* 149, 326–337.
- Moreno, P.I., Villa-Martínez, R., Cárdenas, M.L., Sagredo, E.A., 2012. Deglacial changes of the southern margin of the southern westerly winds revealed by terrestrial records from SW Patagonia (52°S). *Quaternary Science Reviews* 41, 1–21.
- Murdie, R.E., Pugh, D.T., Styles, P., 1998. A lightweight, portable, digital probe for measuring the thermal gradient in shallow water sediments, with examples from Patagonia. *Geo-Marine Letters* 18, 315–320.
- Murray, A., Wintle, A., 2000. Luminescence dating of quartz using an improved single-aliquot regenerative-dose protocol. *Radiation Measurements* 32, 57–73.
- Nimick, D.A., McGrath, D., Mahan, S.A., Friesen, B.A., Leidich, J., 2016. Latest Pleistocene and Holocene glacial events in the Colonia valley, Northern Patagonia Icefield, southern Chile. *Journal of Quaternary Science* 31, 551–564.
- Pedro, J.B., Jochum, M., Buizert, C., He, F., Barker, S., Rasmussen, S.O., 2018. Beyond the bipolar seesaw: Toward a process understanding of interhemispheric coupling. *Quaternary Science Reviews* 192, 27–46.
- Pesce, O.H., Moreno, P.I., 2014. Vegetation, fire and climate change in central-east Isla Grande de Chiloé (43°S) since the Last Glacial Maximum, northwestern Patagonia. *Quaternary Science Reviews* 90, 143–157.

- de Porras, M.E., Maldonado, A., Abarzúa, A.M., Cárdenas, M.L., Francois, J.P., Martel-Cea, A., Stern, C.R., Méndez, C., Reyes, O., 2012. Postglacial vegetation, fire and climate dynamics at Central Chilean Patagonia (Lake Shaman, 44°S). *Quaternary Science Reviews* 50, 71–85.
- de Porras, M.E., Maldonado, A., Quintana, F.A., Martel-Cea, A., Reyes, O., Méndez, C., 2014. Environmental and climatic changes in central Chilean Patagonia since the Late Glacial (Mallín El Embudo, 44°S). *Climate of the Past* 10, 1063–1078.
- Putkonen, J., Swanson, T., 2003. Accuracy of cosmogenic ages for moraines. *Quaternary Research* 59, 255–261.
- Putnam, A.E., Denton, G.H., Schaefer, J.M., Barrell, D.J.A., Andersen, B.G., Finkel, R.C., Schwartz, R., Doughty, A.M., Kaplan, M.R., Schlüchter, C., 2010a. Glacier advance in southern middle-latitudes during the Antarctic Cold Reversal. *Nature Geoscience* 3, 700–704.
- Putnam, A.E., Schaefer, J.M., Barrell, D.J.A., Vandergoes, M., Denton, G.H., Kaplan, M.R., Finkel, R.C., Schwartz, R., Goehring, B.M., Kelley, S.E., 2010b. In situ cosmogenic ^{10}Be production-rate calibration from the Southern Alps, New Zealand. *Quaternary Geochronology* 5, 392–409.
- Ramos, V.A., Kay, S.M., 1992. Southern Patagonian plateau basalts and deformation: Backarc testimony of ridge collisions. *Tectonophysics* 205, 261–282.
- Sagredo, E.A., Kaplan, M.R., Araya, P.S., Lowell, T.V., Aravena, J.C., Moreno, P.I., Kelly, M.A., Schaefer, J.M., 2018. Trans-pacific glacial re-

- sponse to the Antarctic Cold Reversal in the southern mid-latitudes. *Quaternary Science Reviews* 188, 160–166.
- Smedley, R.K., Duller, G., 2013. Optimising the reproducibility of measurements of the post-IR IRSL signal from single-grains of K-feldspar for dating. *Ancient TL* 31, 49–58.
- Smedley, R.K., Glasser, N.F., Duller, G.A.T., 2016. Luminescence dating of glacial advances at Lago Buenos Aires ($\sim 46^{\circ}\text{S}$), Patagonia. *Quaternary Science Reviews* 134, 59–73.
- Smedley, R.K., Pearce, N.J., 2016. Internal U, Th and Rb concentrations of alkali-feldspar grains: Implications for luminescence dating. *Quaternary Geochronology* 35, 16–25.
- Stocker, T.F., Johnsen, S.J., 2003. A minimum thermodynamic model for the bipolar seesaw. *Paleoceanography* 18, 1–9.
- Stone, J.O., 2000. Air pressure and cosmogenic isotope production. *Journal of Geophysical Research: Solid Earth* 105, 23753–23759.
- Strelin, J.A., Denton, G.H., Vandergoes, M.J., Ninnemann, U.S., Putnam, A.E., 2011. Radiocarbon chronology of the late-glacial Puerto Bandera moraines, Southern Patagonian Icefield, Argentina. *Quaternary Science Reviews* 30, 2551–2569.
- Sugden, D., Bentley, M., Fogwill, C., Hulton, N., McCulloch, R., Purves, R., 2005. Lateglacial glacier events in southernmost south america: a blend of northern and 'southern hemispheric climatic signals? *Geografiska Annaler: Series A, Physical Geography* 87, 273–288.

- Thomsen, K., Murray, A., Jain, M., Bøtter-Jensen, L., 2008. Laboratory fading rates of various luminescence signals from feldspar-rich sediment extracts. *Radiation Measurements* 43, 1474–1486.
- Thorndycraft, V.R., Bendle, J.M., Benito, G., Davies, B.J., Sancho, C., Palmer, A.P., Fabel, D., Medialdea, A., Martin, J.R., 2019. Glacial lake evolution and Atlantic-Pacific drainage reversals during deglaciation of the Patagonian Ice Sheet. *Quaternary Science Reviews* 203, 102–127.
- Toggweiler, J.R., Russell, J.L., Carson, S.R., 2006. Midlatitude westerlies, atmospheric CO₂, and climate change during the ice ages. *Paleoceanography* 21, 1–15.
- Turner, K.J., Fogwill, C.J., McCulloch, R.D., Sugden, D.E., 2005. Deglaciation of The Eastern Flank Of The North Patagonian Icefield And Associated Continental-Scale Lake Diversions. *Geografiska Annaler, Series A: Physical Geography* 87, 363–374.
- Veres, D., Bazin, L., Landais, A., Toyé Mahamadou Kele, H., Lemieux-Dudon, B., Parrenin, F., Martinerie, P., Blayo, E., Blunier, T., Capron, E., Chappellaz, J., Rasmussen, S.O., Severi, M., Svensson, A., Vinther, B., Wolff, E.W., 2013. The Antarctic ice core chronology (AICC2012): An optimized multi-parameter and multi-site dating approach for the last 120 thousand years. *Climate of the Past* 9, 1733–1748.
- Villa-Martínez, R., Moreno, P.I., Valenzuela, M.A., 2012. Deglacial and post-glacial vegetation changes on the eastern slopes of the central Patagonian Andes (47°S). *Quaternary Science Reviews* 32, 86–99.

Wenzens, G., 2002. The influence of tectonically derived relief and climate on the extent of the last Glaciation east of the Patagonian ice fields (Argentina, Chile). *Tectonophysics* 345, 329–344.

Wenzens, G., 2005. Glacier advances east of the Southern Andes between the Last Glacial Maximum and 5,000 BP compared with lake terraces of the endorheic Lago Cardiel (49 degrees S, Patagonia, Argentina). *Zeitschrift Fur Geomorphologie* 49, 433–454.